

## Molecular dynamics simulation of atomic friction: A review and guide

Yalin Dong, Qunyang Li, and Ashlie Martini

Citation: *Journal of Vacuum Science & Technology A* **31**, 030801 (2013); doi: 10.1116/1.4794357

View online: <http://dx.doi.org/10.1116/1.4794357>

View Table of Contents: <http://scitation.aip.org/content/avs/journal/jvsta/31/3?ver=pdfcov>

Published by the AVS: Science & Technology of Materials, Interfaces, and Processing

---

### Articles you may be interested in

**Molecular dynamic simulation of tip-polymer interaction in tapping-mode atomic force microscopy**

*J. Appl. Phys.* **114**, 094309 (2013); 10.1063/1.4820256

**The extent of molecular orientation at liquid/vapor interface of pyridine and its alkyl derivatives by molecular dynamics simulation**

*J. Chem. Phys.* **134**, 074707 (2011); 10.1063/1.3554361

**The molecular dynamics simulation of ion-induced ripple growth**

*J. Chem. Phys.* **131**, 204704 (2009); 10.1063/1.3264887

**Elucidating the contact mechanics of aluminum silicon surfaces with Green's function molecular dynamics**

*J. Appl. Phys.* **102**, 113511 (2007); 10.1063/1.2815640

**Atomic indentation and friction of self-assembled monolayers by hybrid molecular simulations**

*J. Chem. Phys.* **113**, 8800 (2000); 10.1063/1.1318223

---



## Instruments for Advanced Science



### Gas Analysis

- dynamic measurement of reaction gas streams
- catalysis and thermal analysis
- molecular beam studies
- dissolved species probes
- fermentation, environmental and ecological studies



### Surface Science

- UHV TPD
- SIMS
- end point detection in ion beam etch
- elemental imaging - surface mapping



### Plasma Diagnostics

- plasma source characterization
- etch and deposition process reaction
- kinetic studies
- analysis of neutral and radical species



### Vacuum Analysis

- partial pressure measurement and control of process gases
- reactive sputter process control
- vacuum diagnostics
- vacuum coating process monitoring

Contact Hiden Analytical for further details:

W [www.HidenAnalytical.com](http://www.HidenAnalytical.com)  
E [info@hiden.co.uk](mailto:info@hiden.co.uk)

**CLICK TO VIEW** our product catalogue

## REVIEW ARTICLE

## Molecular dynamics simulation of atomic friction: A review and guide

Yalin Dong

*School of Mechanical Engineering, Purdue University, West Lafayette, Indiana 47906*

Qunyang Li

*Center for Nano and Micro Mechanics, Applied Mechanics Laboratory, Department of Engineering Mechanics, School of Aerospace, Tsinghua University, Beijing 100084, China*

Ashlie Martini<sup>a)</sup>

*University of California Merced, School of Engineering, Merced, California 95343*

(Received 12 February 2013; accepted 15 February 2013; published 11 March 2013)

This paper reviews recent progress in molecular dynamics simulation of atomic-scale friction measured by an atomic force microscopy. Each section of the review focuses on an individual condition or parameter that affects atomic friction including materials, surfaces, compliance, contact area, normal load, temperature, and velocity. The role each parameter plays is described in the context of both experimental measurements and simulation predictions. In addition, the discussion includes an overview of the research community's current understanding of observed effects, guidelines for implementation of those effects in an atomistic simulation, and suggestions for future research to address open questions. Taken together, this review conveys the message that friction at the atomic scale is affected by many interrelated parameters and that the use of molecular dynamics simulation as a predictive tool can be accomplished only through careful model design. © 2013 American Vacuum Society. [<http://dx.doi.org/10.1116/1.4794357>]

### I. INTRODUCTION

The Amontons–Coulomb law of friction states that the force resisting relative motion between contacting objects, friction, is related to normal load by a constant, the friction coefficient. This relationship has been widely used to describe frictional behavior since its advent in 1699 (Amontons) and 1785 (Coulomb) due to its generality and simplicity. However, despite the success of this phenomenological description, the Amontons–Coulomb law does not capture specific physical processes underlying frictional sliding. Friction has been long recognized as a very complex process, but only recently have measurement technologies and instrumentation been sophisticated enough to enable identification of these complexities. For example, it is now known that contact area evolution is due not only to elastic and plastic deformation but also surface chemistry and environment effects. Understanding these and other factors for a large scale contact is a daunting task. Therefore, many researchers attempt to simplify the problem by focusing on the sliding of a single asperity, where the smallest measurable asperity is usually on the nanoscale. This type of research is also relevant for small scale applications such as MEMS/NEMS or magnetic storage devices where the size of the interface may be on the order of nanometers. In nanoscale contacts, the position and dynamics of discrete atoms can play identifiable roles in determining sliding processes; hence, their sliding resistance is called atomic friction or atomic-scale friction.

<sup>a)</sup>Electronic mail: amartini@ucmerced.edu

The invention of the atomic force microscope (AFM) has enabled quantitative single asperity atomic friction measurements; the first such measurements were reported in 1987.<sup>1</sup> In a typical AFM measurement of friction, a nanoscale tip mounted to a microscale cantilever is pulled to slide against a substrate at a constant normal load as illustrated in Fig. 1(a). The lateral force resulting from the interaction between tip and substrate, usually a few nanoNewtons, causes torsional twisting of the cantilever, which is recorded by an optical method. The tip is moved back and forth across the substrate, resulting in a force contrast pattern called a lateral force image (friction image) such as that shown in Fig. 1(c), or a lateral force trace (friction trace) as shown in Fig. 1(e), which reflect the resistance to sliding as the tip moves over the surface. Due to the atomic discreteness of the surface, the variation of lateral force with displacement is often not smooth but exhibits a saw-tooth pattern that is referred to as stick-slip friction since the tip “sticks” at some position for a while and then abruptly “slips” forward in the direction of lateral forcing. An example of a stick-slip pattern is shown in Fig. 1(e). This type of data can provide quantitative information about the frictional resistance of the surface, energy dissipation, and the correlation between sliding resistance and the atomic structure of the substrate surface.

AFM experiments have helped reveal many new insights associated with atomic friction. However, the instrument itself does not provide direct information about the interface between nanoscale tip and substrate, the so-called buried interface; this hinders interpretation of observed phenomena. To fill this gap, molecular dynamics (MD) simulation has

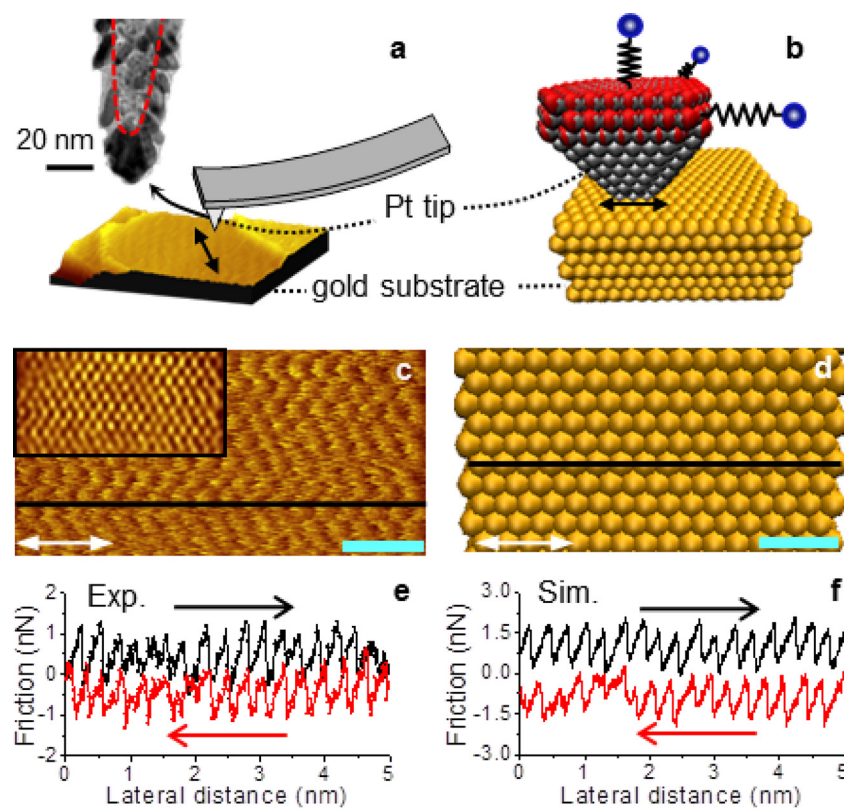


FIG. 1. (Color online) (a) Schematic of an AFM experiment, and a  $100 \times 100 \text{ nm}^2$  topographic AFM image of the Au(111) surface showing large terraces separated by monatomic steps. Inset above: TEM image of the Pt-coated probe. (b) Snapshot of an atomistic tip/substrate model. (c) Lateral force image on Au(111). Inset: Fourier low-pass filtered image. (d) Top view of the model Au(111) substrate. White arrows in (c) and (d) denote the fast scanning direction. Scale bars are 1 nm. (e), (f) Variation of the experimental (e) and simulated (f) lateral force along the horizontal lines shown in (c) and (d), respectively. The simulation and experimental results are obtained under optimally matched conditions: materials Pt/Au(111), incommensurate orientation, effective stiffness 6 N/s, contact area  $7.3 \text{ nm}^2$ , normal load 0.6 nN, and temperature 293 K. Only sliding speeds differ significantly: 149 nm/s in experiment and 1 m/s in simulation (Ref. 2). Reprinted with permission from Li *et al.*, Phys. Rev. Lett. **106**, 026101 (2011). © 2011 by American Physical Society.

been introduced to provide a better understanding of the atomic-scale processes in the buried interface. MD simulation is based on a model that describes the interaction energy between atoms and computes the dynamics of atoms through Newton's Second Law. Thus, in principle, the trajectories of each atom in the model system can be predicted. Further, the correlation between atomic behavior and the collective behavior of the system, in this case atomic friction, can be constructed. Indeed, carrying out MD simulation to complement AFM experiments has become commonplace. Figure 1(b) shows a snapshot of an MD simulation of atomic friction where the model captures the apex of the AFM tip and its interaction with the substrate. The cantilever is introduced in an effective manner through harmonic springs as will be discussed later. A top view of the model substrate is shown in Fig. 1(d). The consistency of the simulation and experimental friction traces shown in Figs. 1(e) and 1(f) illustrates the potential usefulness of a simulation that can not only reproduce experimental measurements, but shed light on the underlying mechanisms. However, realizing this potential requires that the two methods be matched as closely as possible. This matching will be a theme throughout the following sections.

While much effort has been made to review progress in the field of atomic friction,<sup>3–13</sup> this review paper specifically

focuses on how to design a physically representative MD simulation of atomic friction measured by AFM. In the process, we will review the relevant literature and discuss previous results in the context of MD simulation design. The scope of the review will be limited to solid–solid contact in a vacuum environment. Thus, we will not discuss the topics of liquid lubrication, self-assembled monolayers, humidity effects, or the presence of third bodies.

As will be shown in this review, atomic friction is very sensitive to a variety of parameters including materials, surfaces, compliance, contact area, normal load, temperature, and velocity. For an MD simulation to model an AFM experiment, the effect of each of these factors must be understood and properly modeled so it is consistent with the experiment. Facilitating this process is the primary goal of this review. In each of the subsequent sections, we will focus on one influential parameter. Each section will include an overview of that parameter and its effect on friction from both experimental and simulation perspectives, discussion of the mechanisms believed to underly observed effects, guidelines for implementation of that parameter in an MD simulation, and finally suggestions for future research to address open questions. Taken together, these sections are intended to convey the message that friction at the nanoscale is complex and that using MD simulation to reach its full potential

as a predictive tool can be accomplished only through careful model design.

## II. MATERIALS

### A. Overview

Most atomic-scale friction measurements are performed on well-ordered substrate materials so that observed trends can be correlated back to the known atomic structure. The first atomic stick-slip friction was observed on a graphite surface.<sup>1</sup> Graphite is ideal for atomic friction measurements because it can be easily cleaved to render an atomically flat surface with regular crystallographic structure and because it is relatively stable and chemically inert. Since the first measurement on graphite, atomic friction has been measured on many different substrate materials including pure metals, ionic crystals, and various carbon-based materials. Most AFM tips are constructed of silicon, silicon nitride, borosilicate glass, tungsten, or diamond. However, the tip can be coated with different materials to enable a wider variety of measurement possibilities.

Materials are specified in an MD simulation by choosing an empirical model that describes the energetic interaction between the atoms in the system. This model determines the dynamics of atoms leading to the corresponding macroscale material properties. Generally speaking, there is no universal standard with which to judge “good” and “bad” potentials; the choice depends on the purpose of the investigation. The principle is to identify potentials designed to reproduce the desired material properties and then choose the simplest candidate. In this section, we will present several potential models that have been used for atomic friction simulations and discuss the materials for which they are applicable. We will start by describing relatively simple potentials that are often used to capture generic atomic interactions. Then we will focus on potential models specifically designed for three categories of atomic-scale friction materials: metals, covalent materials, and ionic compounds. Finally, we will discuss how the interactions between similar and dissimilar tip and substrate materials can be captured in the model.

### B. Generic potentials

In some cases, simulations are designed to predict the behavior of generic atoms or particles. For these simulations, it is common to employ generic empirical potentials, such as the Lennard-Jones (LJ) model. The concept behind the use of such potentials is that, although real material properties (e.g., elastic or thermal properties) may not be reproduced, the dynamics of the atoms can give insight into how sliding resistance occurs for the general case. They are usually very computationally efficient so large-scale systems can be modeled in a relatively short time.

The LJ potential<sup>14</sup> takes the form of  $V_{LJ} = 4\epsilon[(\frac{\sigma}{r})^{12} - (\frac{\sigma}{r})^6]$ . In this expression, the  $r^{-6}$  term describes the attractive force from the van der Waals interactions, and the  $r^{-12}$  term is intended to simulate the repulsive force originating from Pauli repulsion at a very short distances. However, unlike the  $r^{-6}$  term, the choice of  $r^{-12}$  for repulsive

interactions is empirical; in fact, there are various other forms available, such as  $r^{-9}$  or an exponential.<sup>15</sup> In the LJ formulation, there are two independent parameters, the minimum energy  $\epsilon$  and the zero crossing distance  $\sigma$  (or the minimum energy distance in some implementations), which can be fitted to specific materials. The LJ potential can describe interactions of noble gases well, and as an ideal potential, it is also used to investigate general behaviors of other materials. Many notable discoveries related to atomic friction have been made using the LJ potential; for example, the prediction of the breakdown of continuum contact mechanics at the nanoscale<sup>16,17</sup> and the effect of an adsorbate monolayer on atomic friction.<sup>18</sup> However, because of its simplicity, the LJ potential fails to capture many properties associated with real materials, and extrapolating its result to a specific material requires great care. For simulations intended to produce results that can be quantitatively compared to experiments, one often has to turn to more sophisticated potentials such as those discussed in Sec. II C.

### C. Material-specific potentials

We will discuss three types of materials that are used in atomic friction measurements: metals, covalent materials, and ionic compounds. These three types are differentiated based on their bond properties, and are limiting cases on a van Arkel-Ketelaar or bond triangle.<sup>19</sup> The potential formulations appropriate for each of these types are discussed next.

Metals are a common substrate material in atomic friction studies because of their simple and well-characterized crystallographic structure and ready availability. Typical examples include Au, W, Cu, Al, Pt, Pd, and Ag. Metals are usually characterized by high electron conductivity and thermal transport owing to the fact that the valence electrons in metals can be treated as free electrons. So the interaction between an atom and its surrounding free electrons becomes an essential part of the bonding energy.<sup>20</sup> These properties are described by the Embedded Atom Method (EAM), an empirical potential developed by Baskes and co-workers<sup>21,22</sup> to model metallic systems. EAM looks at the problem from the perspective of total energy and considers two contributions: the interatomic interaction between two atoms and the embedding energy due to the interaction between an atom and the free electron sea. This is expressed by

$$V_{EAM} = F \left[ \sum_{j \neq i} \rho(r_{ij}) \right] + \frac{1}{2} \sum_{j \neq i} \phi(r_{ij}). \quad (1)$$

The first term on the right side is the embedded energy of atom  $i$  in the free electron sea, where the electron sea is a superposition of valence electrons of surrounding atoms indicated by  $j$ , and the second term is the standard pairwise interatomic interaction energy. Thanks to its fundamental description of the metallic system, EAM has been successfully employed to model thermodynamic functions, mechanical behaviors, melting point, defects, grain boundary structure, and frictional behavior (a review of the EAM potential can be found in Ref. 23). Another advantage of this

method is its computational efficiency. Physically speaking, it is a many-body potential, but its computational complexity is on the order of two-body expressions, which enables its application to large-scale problems. Therefore, EAM is an ideal candidate to simulate atomic friction on metals, and it has been applied to study various phenomena associated with atomic friction such as ploughing, cutting, cold welding, junction formation, and clean stick-slip sliding.<sup>2,24–30</sup> One limitation of EAM is that it characterizes metallic bonding as unidirectional. In actuality, only a few metals, such as Mg and Co, have spherically symmetric bonding. To account for this slight deviation from spherical symmetry and thus bond directionality, the Modified Embedded Atom Method (MEAM) was introduced, which adds bonding angles to the EAM potential.<sup>31</sup> Equipped with the ability to simulate geometric effects, MEAM has also been extended to describe semiconducting materials.<sup>31</sup>

Another category of materials used in atomic friction studies is covalent materials. This description covers a vast range of atomic friction materials such as silicon and silicon dioxide, carbon-based materials (graphite, diamond, and diamondlike carbon), organic materials, and many oxides. Covalent bonds are typically formed by valence electrons from two atoms, and the electrons are localized between the two atoms.<sup>20</sup> A covalent bond exhibits two distinguishing characteristics: it is very strong (binding energy ranges from 1 to 5 eV) and it has a marked directional nature.<sup>20</sup> One modeling approach that reflects both characteristics is to explicitly describe the bond based on configurational positions of atoms such that the potential is determined by bond lengths (stretching) and bond angles (bending), and sometimes dihedral angles (torsion). The representative potential is the Stillinger–Weber model, which was initially designed to simulate diamond-structured Si.<sup>32</sup> The idea of viewing bonds from the perspective of length, angle, and torsion not only simplifies the atomic interaction but also enables stabilization of the material structure. The disadvantage of this method stems from the fact that there is only one equilibrium configuration, which means that it cannot capture other stable structures. Bond-order potentials were invented to address this limitation by introducing a bond-order parameter to evaluate the strength of different bonds so that stable states associated with different bonds could be described simultaneously by one potential. However, because they take more parameters into consideration, the bond-order potentials are very computationally intensive and parallel implementations are often needed. Representative bond-order potentials include Tersoff,<sup>33</sup> which was initially formulated for Si and then extended to other solid state structures, the reactive empirical bond-order (REBO) potential developed by Brenner,<sup>34</sup> an extension of Brenner's potential for hydrocarbon molecule systems called adaptive intermolecular REBO (AIREBO),<sup>35</sup> which includes long-range atomic interactions and single bond torsional interactions, and ReaxFF,<sup>36</sup> which has been parameterized for a variety of materials including polymers, ceramics, and metals. Numerous MD simulations of friction have been conducted on materials utilizing these types of potentials.<sup>37–41</sup>

The last material group used in atomic friction studies that we will mention is ionic compounds in which the dominant form of bonding is ionic. These materials usually consist two or more oppositely charged ions. Typically, the positively charged ions are metal elements and negatively charged ions are halogens. Ionic compounds are useful for measuring atomic friction because, like metals, they are crystallographically simple and readily available. Ionic materials commonly used in friction studies are NaCl (Refs. 42–44) and KBr.<sup>44,45</sup> To physically represent the ionic bond in a model, one needs charge-based interatomic potentials described by the long-range Coulomb force. However, long-range interactions significantly increase computational time, which limits the size and duration of MD simulations. Although direct simulation of friction on ionic compounds is rare, there have been some efforts. For example, atomic friction of KBr was modeled<sup>46</sup> through a combination of the short range Buckingham and Coulomb potentials with each ion modeled as a spring-coupled system of positively charged core and negatively charged shell (the shell model). We anticipate that, as experimental measurements continue to be taken on ionic compounds, more simulations will be developed to complement them.

#### D. Tip–substrate interactions

In Sec. II C, we focused on atomic interactions within a given material. An atomic friction system consists of a tip and substrate, which may not be the same material. MD simulations must be able to accurately capture this interaction in order to realistically describe sliding friction, especially for cases where most of the resistance to sliding comes from the tip–substrate energetic interaction (as opposed to the physical interlocking atomic asperities or wear).

In some rare cases, it has been reported that the tip picks up material from the substrate during its initial contact.<sup>47–49</sup> If we assume this occurs, we can model a sliding interface within the substrate material, which means the same potential can be used for all atomic interactions in the system. However, if the tip and substrate are different materials, which is often the case in an AFM experiment, the model must include a so-called cross-potential that describes the interaction between dissimilar atoms. If the tip and substrate are similar material types, then the cross potential may already be well-defined. For example, EAM potentials that accurately describe the interaction between many different metals are available [e.g., Ag–Cu (Ref. 50) and Cu–Al (Ref. 51)]. However, issues can arise when the best potential form for the tip is not the same as that for the substrate. For example, a metal-coated tip may be modeled using EAM while the graphite substrate on which it slides is best modeled using AIREBO. In this case, researchers often rely on the Lennard–Jones model to describe tip–substrate interactions. Lennard–Jones parameters for dissimilar atoms can be obtained using the Lorentz–Berthelot mixing rules. If the frictional behavior of the system is dominated by van der Waals interactions with no severe wear, the results predicted by a model with an LJ tip–substrate interaction may be

qualitatively sound. However, if that is not the case, one may have to develop a more accurate cross potential.

### E. Summary and outlook

In summary, atomic friction is affected by the material of the tip and substrate, so reliably capturing the properties of those materials through accurate empirical potentials is critical to predicting physically-realistic atomic friction. Atomic friction measurements are now performed on a variety of materials, from wear-resistant materials such as diamond, to materials with strong adhesion and wear such as metals. Therefore, MD simulations require a wide variety of interaction potentials to be able to accurately describe experimentally-measured friction. Particularly challenging is capturing interactions between dissimilar materials. This has been partially addressed by potentials that are intentionally designed to model chemically diverse materials. A good example of this is the charge-optimized many body (COMB) potential, which enables simultaneous modeling of interactions between metals, oxides, and covalently bonded structures.<sup>52,53</sup> The ReaxFF potential<sup>36</sup> has also been parameterized for a diverse set of materials. We anticipate that these generally-applicable models will continue to be developed and will facilitate simulations of atomic friction for more and more varied interfaces. This process will be facilitated by the emergence of first principles calculations, which can provide the reference data necessary for fitting empirical models.

The availability of more potentials has also introduced a new challenge: researchers now need to be able to effectively and efficiently evaluate the accuracy of published potential parameters. Several recent attempts have been made to address this issue by developing repositories of potentials that have been, at least nominally, vetted for their accuracy and reliability. For example, the Interatomic Potential Repository Project is a publicly accessible online list of potentials maintained by the National Institute of Standards and Technology (NIST).<sup>54</sup> Another project, the Knowledgebase of Interatomic Models (KIM), aimed at developing an online source for standardizing testing and long-term warehousing of interatomic models, is also underway.<sup>55</sup> These types of efforts will hopefully make development of atomic friction simulations more flexible and efficient for a wider variety of realistic materials.

## III. SURFACES

### A. Overview

In Sec. II, we discussed modeling of specific materials. Now we will extend this discussion to consider the surfaces of those materials. Interface features can have a significant effect on how two surfaces slide relative to one another and the resulting friction. At the atomic scale, lattice structure and other surface characteristics can result in distinct energetic landscapes and thus identifiable friction patterns.<sup>16</sup> In addition, the relationship between the contacting tip and substrate surface structures can affect friction. A controlled way to vary the relative surface structure is to rotate the tip with

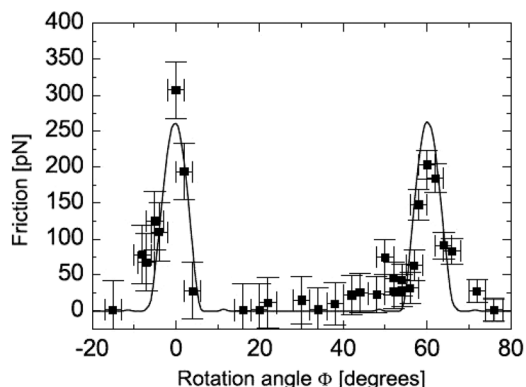


FIG. 2. AFM measurement of mean friction as a function of rotation angle between graphite surfaces. The highest friction occurs in aligned contact ( $0^\circ$  and  $60^\circ$ ) (Ref. 48). Reprinted with permission from Dienwiebel *et al.*, Phys. Rev. Lett. **92**, 126101 (2004). © 2004 by American Physical Society.

respect to the substrate and analyze friction as a function of orientation. For example, Fig. 2 (Ref. 48) demonstrates that friction can vary significantly with the relative orientation of two graphite surfaces in contact. This result shows that high friction occurs when the tip and substrate lattices are aligned ( $0^\circ$  and  $60^\circ$ ) while low friction is exhibited in misaligned contact. Note that we use the terms aligned and misaligned here, which are more flexible than the sometimes-used commensurate and incommensurate to enable discussion of orientation effects between slightly dissimilar surfaces.

In this section, we will discuss the effect of surfaces on friction. The energetics of different surfaces will be shown to play a major role in how sliding happens on metals. In addition, the effects of longer range surface features will be discussed. We will also explore the role of orientation, which affects not only the magnitude of measured friction but also the way the tip slips over the substrate. This behavior will be discussed in terms of MD-predicted atomic position and stress distributions in the contact area. Finally, we will discuss considerations associated with designing an MD simulation with physically realistic surfaces and relative surface orientation.

### B. Substrate surface

The surface of the substrate plays a significant role in determining atomic friction. This is particularly true for metals on which both MD simulation and AFM measurements reveal that cold welding and strong adhesion are dominant on high energy surfaces, while low energy surfaces, e.g., the (111) surface for face centered cubic (FCC) metals, are associated with stable, stick-slip sliding.<sup>47,49,56</sup> As an example, friction on two representative surfaces of Au obtained from MD simulation is shown in Fig. 3. In Fig. 3(a), the strong adhesion of the Au(100) surface dominates the process and an atomic interface junction forms. As a result, the apex of the tip is worn off as shown in the inset snapshots and no stable friction force is acquired. This is similar to what has been observed on model Cu(100)<sup>56</sup> and is consistent with experimental measurements on high-energy metal surfaces.<sup>47,49</sup> In contrast, Fig. 3(b) demonstrates the very regular sawtooth-

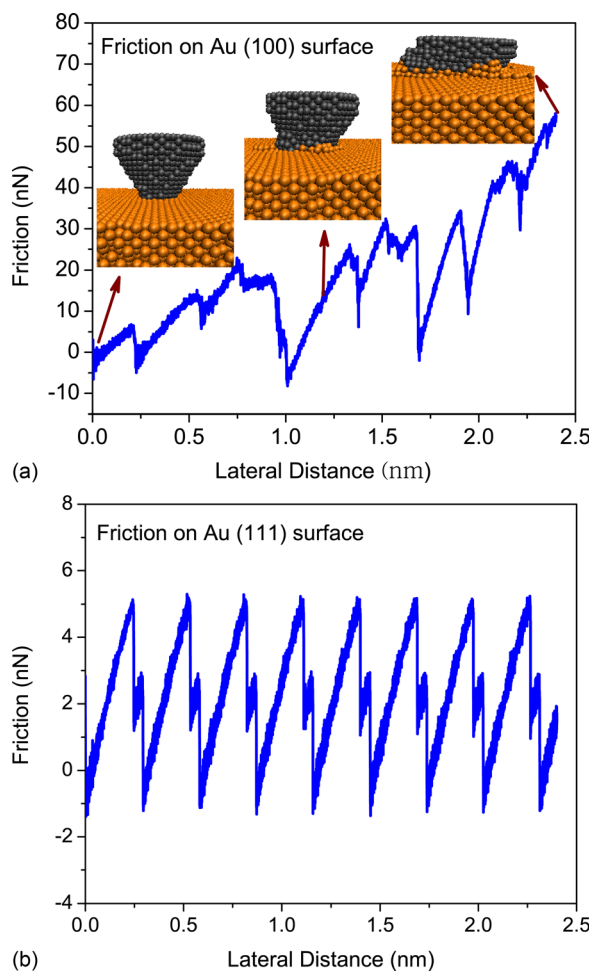


FIG. 3. (Color online) Friction from a Pt tip sliding on the (a) Au(100) and (b) Au(111) surfaces from MD simulation. In (a) the Pt tip is worn off almost immediately due to junction formation and no stable friction pattern observed while in (b) a stable bimetallic interface forms and regular stick-slip friction arises. Note that the scales of the y-axes differ in the two plots. Simulation parameters: EAM potential, load 0 nN, temperature 10 K, speed 1 m/s, and contact area  $1.2 \text{ nm}^2$  (aligned).

like lateral force as a function of lateral distance obtained from simulation of sliding on the low energy Au(111). This explains why essentially all stable stick-slip observed in AFM measurements on metal surfaces have been conducted on the (111) surface of FCC metals<sup>2,30,47,49</sup> and most simulations are designed correspondingly.<sup>30,56,57</sup>

Some materials exhibit longer range (larger than the atomic lattice) surface features, which also affect friction. For example, herringbone reconstruction on the Au(111) surface<sup>58</sup> has been shown to modulate friction in distinct ways.<sup>44,59–61</sup> The empirical potentials described in Sec. II have been shown to predict bulk material properties well but are sometimes unable to predict structural features that are unique to surfaces. For metals, the most commonly used potential, EAM, is known to underestimate surface energy<sup>50</sup> and therefore may not be able to capture associated surface features. To address this issue in an atomic friction model, one can apply an EAM parameter set that has been fitted specifically to reproduce surface features<sup>62</sup> or a known surface feature can be artificially introduced into the atomistic

model. An example of the latter approach is manually positioning the gold atoms on a model substrate to reproduce Au (111) surface reconstruction. This method enabled an MD simulation to predict friction behavior that was qualitatively consistent with AFM measurements.<sup>61</sup>

Another topographic feature ubiquitously exhibited on surfaces of ordered materials is the atomic step edge, where the uppermost layer of atoms begins or ends. This affects friction in different ways depending if the AFM tip is moving up or down the step. When the tip slides up a step edge, measurements and simulations have shown that there is always an enhanced resistive force at the step.<sup>63–67</sup> At step-down, AFM experiments have shown two contrasting trends: The lateral force can either assist<sup>65</sup> or resist<sup>66</sup> the tip's motion. The conflicting trends have been attributed to the competition between geometric and energetic effects<sup>68,69</sup> where geometry assists the tip while an energetic barrier due to the presence of the step provides resistance. Simulations can be used to help understand these trends if the surface features are accurately introduced into the model.

### C. Orientation

It is now well-known that the relative positions of atoms in the buried interface between the tip and substrate play a significant role in atomic-scale friction. The forces in the interface are usually not uniformly distributed. We can imagine that, at any given time, some atoms in the buried interface will experience a forward force (in the sliding direction), while others experience a backward force (opposite to the direction of sliding). If the conditions are such that the interaction forces in different directions counteract each other, then the net total force is small as is observed for misaligned contact. This can also be viewed from an energetic perspective: misaligned surfaces correspond to shallower energy basins and therefore less resistance to sliding. The resulting low friction state has been called “superlubricity.”<sup>70</sup> Since this is entirely a structural effect, Müser suggested the term structural lubricity to differentiate it from superconductivity (which is a quantum effect).<sup>71</sup> Structural lubricity has been experimentally observed on many different materials including MoS<sub>2</sub>,<sup>72</sup> Si/W,<sup>73</sup> Ti<sub>3</sub>SiC<sub>2</sub>,<sup>74</sup> and graphite.<sup>48</sup> However, a prerequisite for structural lubricity is that there is no wear stemming from either chemical reactions or cold welding, and the bulk hardness within the tip and substrate is much stronger than the interfacial interaction.<sup>71</sup> So structural lubricity is usually achieved under low normal loads and between two chemically-inert materials. Even though structural lubricity is not achieved under all conditions, orientation between the tip and substrate can still affect frictional behavior and is therefore an important factor when designing an MD simulation.

MD simulations explicitly describe atoms in both the tip and substrate and so can capture the effect of relative surface structures. In Fig. 3(b), we show sliding between Pt(111)/Au(111) surfaces yields stable stick-slip with no cold welding. Since both Au and Pt have FCC structures and similar lattice spacings (0.3920 nm for Pt and 0.4080 nm for Au), the friction at this interface is likely to be affected

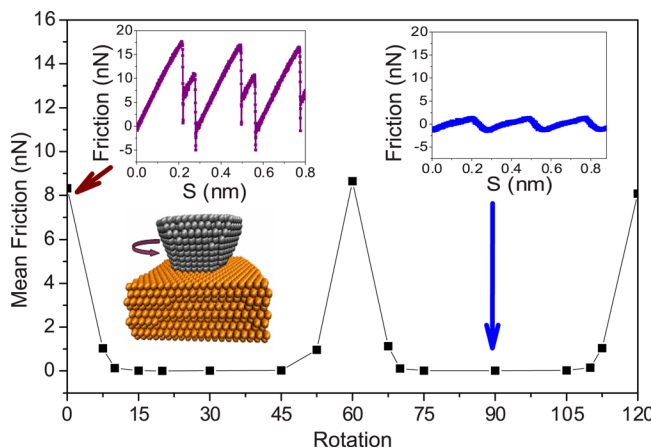


FIG. 4. (Color online) MD simulation of mean friction as a function of rotation angle between Pt(111) tip and Au(111) substrate. Due to the similar lattice constants ( $a_{Pt} = 0.3920 \text{ nm}$  and  $a_{Au} = 0.408 \text{ nm}$ ) and FCC structure of both materials, high friction arises at aligned contact and low friction at misaligned contact. Inset: representative friction traces at aligned and misaligned contact, where  $S$  is the position of the support. Simulation parameters: EAM potential, load 0 nN, temperature 10 K, speed 1 m/s, and contact area  $7.3 \text{ nm}^2$ .

significantly by orientation. This effect is shown in Fig. 4 where alignment of the tip and substrate lattices (relative rotation of  $N \times 60^\circ$  where  $N$  is an integer) corresponds to large friction while misalignment (deviation even a few degrees from aligned contact) causes the friction to drop rapidly. This trend is consistent with the experimental results shown in Fig. 2.<sup>48</sup>

To understand the connection between structure and friction, we can use MD to look at the positions of the atoms and the resulting stress distribution in the contact area. For the same Pt(111)/Au(111) interface discussed above, the tip

and substrate atoms in the contact region form a superstructure, Moiré pattern, as shown in upper images of Fig. 5. The shape of the pattern can be characterized quantitatively based on the relative rotation angle  $\theta$  and the nearest atom distance on the surface  $L$  (assuming the tip and substrate share the same lattice constant). The periodicity  $P$  of the superstructure is given by<sup>75,76</sup>

$$P = \frac{L}{2\sin(\theta/2)}. \quad (2)$$

These patterns can be related to the friction force by calculating the virial stress. As shown in the lower half of Fig. 5, the shear stress distributions exhibit a pattern similar to the Moiré pattern formed by the atoms. The homogeneous shear stress distribution only arises in aligned contact ( $0^\circ$  in this case). In misaligned contacts ( $15^\circ$  or  $30^\circ$ ), positive and negative shear stresses exist simultaneously resulting in low friction.

Orientation and surface structure also affect how slip happens. The simplest picture of slip is the collective uniform motion of atoms in the direction of sliding. However, this concept becomes inadequate when structure and stress inhomogeneity are considered. If the tip and substrate surfaces are not perfectly aligned, stress inhomogeneity could cause partial slip in which a subset of the contacting surface moves first;<sup>56,57,77</sup> partial slip is in contrast to uniform slip where all the atoms in the contact move forward at once. Further, the displacement of the atoms coincides with the accumulation or relief of the shear stress, which implies that structural inhomogeneity is directly related to partial slip. Hence, it is appropriate to describe slip as a dislocation-assisted process.

The concept of “partial slip” is not new and has its origins in continuum mechanics.<sup>78–80</sup> To study this effect with

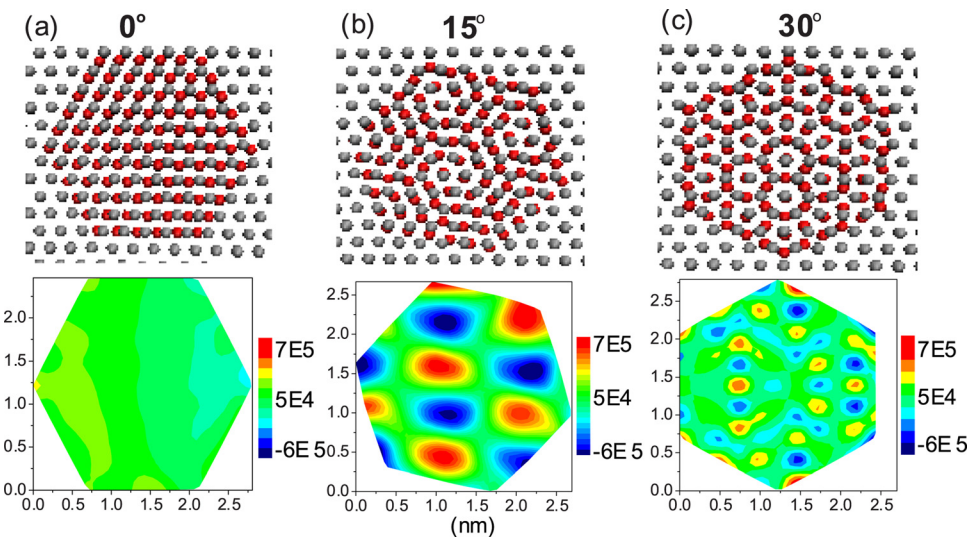


FIG. 5. (Color online) Upper images: Atomic distribution in the buried interface (top) where the light-colored dots are substrate atoms and the dark-color dots are tip atoms. The relative rotation of the surfaces forms superstructures called Moiré patterns. Lower images: Shear stress (color scale in units of bar  $\times \text{Å}^3$ ) distribution of the atoms in the lowermost layer of the tip. Atom and stress distributions shown at relative rotation angles of (a)  $0^\circ$ , (b)  $15^\circ$ , and (c)  $30^\circ$ . Simulation parameters: EAM potential, load 0 nN, temperature 10 K, speed 1 m/s, and contact area  $7.3 \text{ nm}^2$  (Ref. 57). Reprinted with permission from Dong *et al.*, Modeling Simul. Mater. Eng. **19**, 065003. © 2011 IOP Publishing.

atomic level detail, Marks *et al.* incorporated the theory of interfaces, contact and dislocations to theoretically interpret experiments.<sup>75</sup> A similar effort used a theoretical approach which predicted stress concentrations at the periphery of the contact due to dislocations and stress concentrations within the contact due to structure.<sup>81</sup> Note that the extent to which atomic friction depends on orientation and the importance of dislocation-assisted slip is dependent on the materials. As mentioned previously, if wear dominates the process, the orientation effect may be limited. In addition, it tends to be more difficult to induce dislocation-like slip for harder materials in which case uniform slip may still be a good assumption.

Surface structure affects friction not only through the orientation of the two surfaces, but also through the direction the sliding occurs relative to those structures. This anisotropy has been measured both in simulations and experiments on a variety of materials.<sup>37,82–86</sup> The results can be understood generally in terms of the anisotropic energy landscape stemming from the lattice structure. Driven by an external force, the tip tends to take the lowest energy path available. Because a 2D profile of the energy landscape differs depending on the direction from which the profile is taken, the magnitude as well as the periodicity of friction is dependent on sliding direction. This argument is similar to the one used in the discussion of structural lubricity; in both cases, surface features affect the energetic landscape, which in turn determines the frictional resistance to sliding.

#### D. Model considerations

We have shown in this section that friction can be significantly affected by the relative orientation of the sliding surfaces and the direction of sliding. This leads to the question of what orientation and sliding direction should be prescribed in an MD simulation. The challenge is that, although the crystallographic structure of the substrate in an experiment is measurable, it is extremely difficult to determine the atomic structure of the tip surface during sliding. To address this in a simulation, it is necessary to make assumptions. In an experiment, the tip is not necessarily flat so perfect alignment is unexpected to occur by chance (though experiments can be designed explicitly to capture commensurability<sup>48</sup>). In addition, as shown in Fig. 4, simulations show that the high friction of aligned contact is the exception, only occurring for a very limited range of relative orientations. Therefore, unless deliberately arranged, we believe perfectly aligned contact is rare in experimental measurements of atomic friction.<sup>2</sup> So, for designing a realistic MD simulation, it is usually recommended to model misaligned contact unless the goal is to match an experiment already known to be measuring aligned friction.

#### E. Summary and outlook

In summary, the characteristics of contacting surfaces directly affect both the magnitude of friction and the underlying mechanisms. It is therefore important to capture surface characteristics in the model as realistically as possible. However, this remains a challenge for modelers because of

limitations in the information available from experiments and limitations inherent in the simulations themselves.

Real surfaces are rarely perfect crystals, and these imperfections will certainly affect measured friction. Therefore, an MD simulation designed to complement that experiment ideally should include all surface features. This, of course, is a challenge because AFM experiments cannot currently provide atom-by-atom information about the sliding surfaces. The tip apex in particular is an issue because even its size and shape are often unknown. This encourages the integration of alternative techniques, for example, atom probe tomography (APT), which can interrogate the material structure and chemistry of the near apex regions of commercial tips.<sup>87</sup> Modelers should pay attention as such techniques become more common and take advantage of the new information available to improve the accuracy of the simulation and better capture the atom-scale features of a sliding interface.

Assuming we have sufficient information about a given surface, modeling efforts are also limited in their ability to capture large-scale phenomena. As discussed in this section, misalignment between two crystalline surfaces can lead to suppression of atomic friction because of the structure-induced stress inhomogeneity in the interface. When the interfacial interaction between tip and substrate is comparable to the hardness within the tip or substrate, stress inhomogeneity causes the slip process to become more complicated: Instead of atoms moving in concert, slip occurs through dislocation-like motion. One limitation to using models to understand these processes has been that modeling dislocations requires relatively large simulations. This precludes direct modeling of phenomena that occur over larger length-scales as well as investigation of size effects. With currently available optimized MD codes and faster-than-ever computers to run them on, we anticipate more research in this area.

## IV. COMPLIANCE

#### A. Overview

Since an AFM measurement system is not rigid, any force will result in deformation. The relationship between force and deformation is quantified by the stiffness constant. For AFM operated in lateral force mode, the lateral stiffness, which is defined as the force needed to move the tip through a unit displacement in the sliding direction, is an important parameter. The total effective lateral stiffness  $k_{\text{eff}}$  can be directly measured from the approximately linear slope of the lateral force versus displacement curve during the stick phase of the stick-slip process. The typical effective stiffness of AFM measurements has been reported to be around  $1 \sim 10 \text{ N/m}$ .<sup>42,43,45,47,88</sup>

The lateral stiffness directly affects the magnitude of the mean friction acquired from AFM measurements. It is also an important factor in determining transitions between friction regimes from smooth sliding to single, and multiple slips.<sup>43,89,90</sup> There are multiple contributions to the effective stiffness of the system and recognition of each of these

contributions has been a gradual process that has spanned decades. In this section, we will discuss the meaning of each contribution and then describe how or if they can be effectively captured in an MD simulation.

## B. Contributions to lateral stiffness

The discussion of contributions to the lateral stiffness in AFM measurements in the context of atomic friction starts with the seminal work of Carpick *et al.*,<sup>91</sup> in which the effective stiffness of an AFM system was proposed to consist of two components:

$$\frac{1}{k_{\text{eff}}} = \frac{1}{k_{\text{lever}}} + \frac{1}{k_{\text{contact}}^*}, \quad (3)$$

where  $k_{\text{lever}}$  is the stiffness of the micro-fabricated cantilever and the contact stiffness  $k_{\text{contact}}^*$  is defined as the amount of force per unit displacement required to elastically deform the material in the contact region.<sup>91</sup>

The stiffness of the cantilever  $k_{\text{lever}}$  has been recognized since the invention of AFM (Ref. 92) as essential to the use of the mechanical probe for measuring atomic-scale interactions. The lateral stiffness of a cantilever is associated with its torsional motion and is usually calculated as the torsional spring constant divided by tip height.<sup>93</sup> In general, the torsional spring constant depends on the geometry of the cantilever (e.g., shape, length, and thickness) as well as the elastic properties of the comprising material(s). The torsional spring constant can be measured experimentally by calibration procedures or can be estimated from analytical models or numerical simulations.<sup>94</sup> The typical value of lateral stiffness of a cantilever ranges from tens to hundreds of N/m for commercial contact-mode probes.<sup>95–97</sup>

The contact stiffness  $k_{\text{contact}}^*$  in Eq. (3) is associated with the remainder of the stiffness contributions except that from the cantilever. It has been proposed that this stiffness can be estimated in the framework of contact mechanics (see Fig. 6) by the relation  $k_{\text{contact}}^* = 8Ga$ ,<sup>91,96,98</sup> where  $G = ((2 - \nu_1)/G_1 + (2 - \nu_2)/G_2)^{-1}$  is the effective shear modulus combining the two materials of the tip and substrate ( $\nu$  and  $G$  are

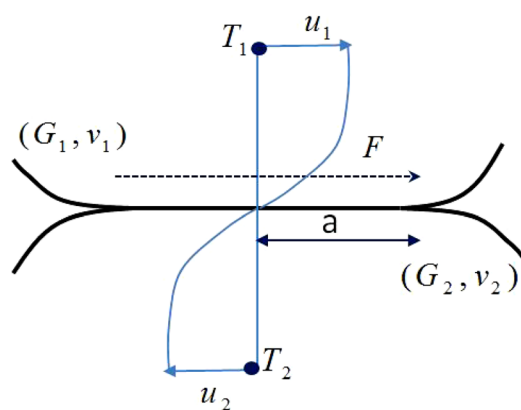


Fig. 6. (Color online) Schematic illustration of the elastic contact between spherical bodies used to derive an expression for contact stiffness in the framework of contact mechanics. Variables are defined in the text.

Poisson's ratio and shear modulus, respectively), and  $a$  is the radius of the contact area. It is important to note that this equation assumes that continuum mechanics is valid at the scale of the single asperity, the radius of the tip is much larger than the radius of the contact area, the deformation is elastic, and that there is no relative motion between the tip and the substrate.<sup>78</sup> In addition, the expression for contact stiffness in Eq. (3) includes the stiffness of the tip apex as well as that of the contact because it is derived from  $k_{\text{contact}}^* = \frac{F}{u_1 - u_2} = 8Ga$ , where  $F$  is the lateral force and  $u_1$  and  $u_2$  are the displacements of two points far from the contact in the tip and substrate where the strain profile is approximately constant, as shown in Fig. 6.

Since the introduction of the two-contribution stiffness model [Eq. (3)], additional contributions have been proposed. It has been suggested that, instead of the single term  $k_{\text{contact}}^*$ , there are separate contributions to the effective stiffness from the main body of the tip  $k_{\text{tip}}$ , the nano-sized tip apex  $k_{\text{apex}}$ , and the contact stiffness due to interaction between the tip and substrate  $k_{\text{contact}}$ . This relationship can be summarized by the equation below:

$$\frac{1}{k_{\text{eff}}} = \frac{1}{k_{\text{lever}}} + \frac{1}{k_{\text{tip}}} + \frac{1}{k_{\text{apex}}} + \frac{1}{k_{\text{contact}}}. \quad (4)$$

Each of the three new terms will now be discussed.

Although the tip is connected to the cantilever, it is not explicitly considered in calibrations of the cantilever stiffness. It is therefore believed that the tip will contribute to the stiffness of the system independently. Lantz *et al.* utilized the finite element method to calculate the stiffness of a typical AFM tip, whose geometrical parameters were measured through TEM (transmission electron microscopy) images and using the bulk material properties of silicon and silicon nitride.<sup>91,96,98</sup> They concluded that the stiffness of the tip is on the same order as the stiffness of the cantilever. Since both the cantilever and tip stiffness are much larger than the effective stiffness measured experimentally, this suggests that the dominant contribution to the overall stiffness of the system should come from one of the two remaining terms, the tip apex or the contact stiffness.

In Eq. (4), we have isolated the stiffness of the tip apex from that of the main body of the tip. It has been proposed that the tip apex is in fact more compliant than the main body of the tip.<sup>99–103</sup> This assumption is based on the argument that the nanoscale sharpness of the tip should correspond to greater compliance. The introduction of the tip apex flexibility as an independent contribution to the overall stiffness has significantly enriched the physical complexity of atomic friction, and has been used to interpret the fine structures and elongated slip duration in atomic friction.<sup>45,99–101,104</sup>

With the tip apex stiffness considered a distinct contribution, the contact stiffness is associated with two types of displacement: the slow sliding between the tip and substrate in the stick phase of stick-slip and the deformation of the substrate. However, it is difficult to quantify the stiffness of either of these two displacement modes. One might consider

the strength of interatomic bonds to analyze slow sliding, or apply a continuum mechanics argument for the substrate deformation. However, at this point, there are no convincing quantitative methods for estimating contact stiffness or for differentiating the contributions due to the contact and tip apex.

### C. Model considerations

Next we focus on how to model AFM stiffness effectively in MD simulations. It is well known that, since MD simulation calculates the dynamics and trajectories of all atoms, there is a limit to the number of atoms (millions) that can be explicitly described in the model. Compared to the actual AFM system, millions of atoms can only simulate a small portion of the tip apex and the contact itself. Therefore, the stiffness of the microscopic main body of the tip and the cantilever has to be introduced artificially. The common approach is to introduce the contributions of stiffness that are not explicitly described by the atoms in the simulation through harmonic springs.<sup>2,105–111</sup> A typical MD simulation setup is illustrated in Fig. 7, where harmonic springs in each of the three directions connect the atoms in the topmost layers of the tip apex (often treated as a rigid body) to supports. In the  $x$ -direction, the support moves at a constant speed such that the lateral force in the  $x$ -direction is the friction.

The stiffness of the spring in the normal direction  $k_z$  can be directly set to that of the AFM cantilever since it will be the most compliant part of the system in that direction. The typical normal stiffness of the micro-cantilever used in measurement of atomic friction is in the range of 0.01–1 N/m.<sup>91</sup> However, there are additional considerations for a model. First, to eliminate the rotational instability of the system, the rotational freedom of the layers of atoms at the top of the tip that are connected to springs needs to be restricted. Second, the very low stiffness at normal direction may cause artificial oscillation in some simulations. Note that these instabilities are artifacts of the simulation; they do not arise in an experiment due to large mass of the microscale cantilever and tip. To address this issue in the model, one may either set a very

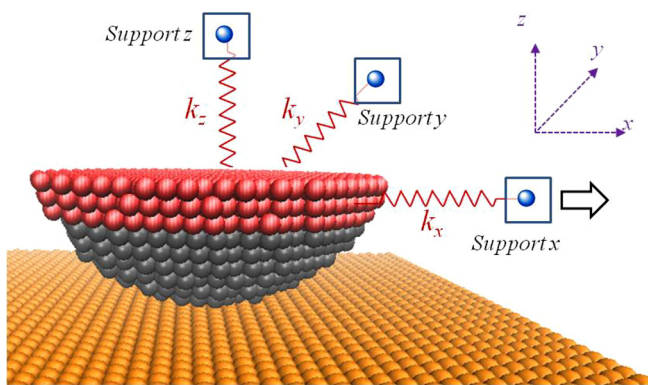


Fig. 7. (Color online) Illustration of an MD simulation with compliance introduced through three harmonic springs ( $k_x$ ,  $k_y$ , and  $k_z$ ) connected to the top layers of the tip apex. Along the  $x$ -direction, the support moves at contact speed to drag the tip apex to slide against the substrate.

large normal stiffness to the spring and apply the normal load to the virtual atom, or eliminate the normal spring/virtual atom and apply the normal load directly to the rigid top layers of the tip apex. From our experience, this choice has little effect on the resulting model-predicted friction force.<sup>111</sup>

The remaining question is how to choose the stiffness of the harmonic springs in the lateral directions. Although the discussion in this section has been focused on the lateral stiffness in the direction of sliding  $k_x$ , it is common practice to set the stiffness of the spring in the transverse lateral direction  $k_y$  to the same value. For the simulation cases we have performed, the effect of  $k_y$  is minimal.

Finally, we consider how to select  $k_x$ . One approach is to simply set  $k_x$  to be the same as that of the cantilever.<sup>105,107,108</sup> However, based on the understanding that the cantilever is not the only source of system stiffness (i.e., the main body and apex of the tip contribute), a more accurate approach is to specify the spring stiffness directly such that the simulated effective stiffness is equal to the experimental effective stiffness,  $k_{\text{eff,AFM}} = k_{\text{eff,MD}}$ .<sup>2,106,109,110</sup> To design such a simulation, one therefore needs to select a lateral spring stiffness that captures the difference between the effective stiffness from experiment and what is described explicitly in the model (i.e., stiffness due to atoms in the contact and a small portion of the tip apex). Given a target effective stiffness, to determine the spring stiffness that should be used in the simulation, one needs to approximate the model stiffness  $k_{\text{atoms}}$ , where  $k_{\text{atoms}}$  is the stiffness due to the atoms explicitly included in the model. This can be done by simply choosing a value of  $k_{x,\text{test}}$  and running the simulation; the model stiffness is then simply  $k_{\text{atoms}} = (\frac{1}{k_{\text{eff,test}}} - \frac{1}{k_{x,\text{test}}})^{-1}$ , where  $k_{\text{eff,test}}$  is the slope of the resulting simulation-predicted force trace. The spring stiffness that should be prescribed for an accurate effective simulation stiffness is then simply calculated from  $k_x = (\frac{1}{k_{\text{eff,AFM}}} - \frac{1}{k_{\text{atoms}}})^{-1}$ . Alternatively, one can simply vary the spring stiffness iteratively until the desired effective stiffness is obtained. However, the former method gives more insight into the physical nature of the stiffness described by the model. Note also that the effective stiffness increases with normal load.<sup>91,96</sup> If the structural evolution of the tip apex and contact with normal load are negligible or perfectly captured by the simulation, then there is no need to adjust the model stiffness to accommodate different loads. However, it is important to be aware that load can affect stiffness and account for this variation if necessary.

### D. Summary and outlook

This section contained a description of the various contributions to compliance in an AFM experiment and then how to best capture the overall effective stiffness in an MD simulation. However, there are still many unanswered questions related to compliance. For example, how should the stiffness of the tip apex and the stiffness of the contact be differentiated? Also, how do the tip apex and contact change structurally with the normal load and what effect does this have on stiffness? These questions encourage more sophisticated

experiments such as *in-situ* TEM.<sup>112–114</sup> For example, real-time monitoring showed that the gold/gold interface under low normal load may form junctions that behave like a liquid.<sup>113</sup> On the other hand, under high normal loads, sliding at a tungsten/gold interface was found to be dominated by dislocations and wear.<sup>112</sup> The discrepancy in the two experiments implies that the tip stiffness depends on material and can span a large range of values. MD simulation with carefully prescribed stiffness can be used to understand these types of discrepancies.

As the size-scale limitation of MD simulation precludes the full compliance of the AFM system from being included in the model, the spring method presented here is currently the state of the art. However, to truly match simulation and experiment, a multiscale model may need to be introduced that describes the atomistic detail of the interface using MD and the dynamics of the cantilever and tip using a continuum or other coarse-graining approach. Such a model would enable direct matching of each of the contributions to compliance and, in conjunction with the direct experimental observations described in the previous paragraph, could enrich our understanding and interpretation of the role of compliance in atomic-scale friction.

## V. CONTACT AREA

### A. Overview

At the macroscale, contact size is quantified as either real or apparent contact area. The real contact area is a small subset of the apparent contact area where asperities are in direct contact and that supports the load. AFM measurements are intended to capture the sliding of a single asperity so the distinction between real and apparent area is vague. Therefore, it is typical to simply use the general term contact area when analyzing atomic friction. Both simulations and experiments of single asperity sliding have shown that friction is affected by contact area. This is, of course, interrelated with the effect of load, which will be discussed in Sec. VI.

Before we can characterize the effect of area, we have to first determine how to quantify area for nanoscale contacts. We will briefly review continuum mechanics estimates of contact area. Then, based on MD predictions of contact area

that suggest continuum theories may not be applicable for some atomic-scale contacts, an alternative definition of contact based on atom–atom distance will be presented. We will next discuss how friction varies with area for a given definition of contact area. As shown in Fig. 8,<sup>115</sup> the effect that area on friction can differ significantly from case to case. The origin of this variation will be explored. Finally, we will describe how to approximate contact area in an MD simulation and best model an experiment where the size and shape of the contact area during sliding are usually not known.

### B. Defining contact area

In the framework of continuum mechanics, the contact area  $A$  increases with normal load and the rate of this increase can be estimated as a function of material properties. For elastic contact between two spherical bodies without adhesion, Hertz theory predicts the contact area as<sup>116</sup>

$$A = \pi \left( \frac{RN}{E^*} \right)^{2/3}, \quad (5)$$

where  $N$  is the normal load,  $R = \frac{R_1 R_2}{R_1 + R_2}$  is the effective radius, and  $E^* = \frac{4}{3}((1 - \nu_1^2)/E_1 + (1 - \nu_2^2)/E_2)$  describes the effective elastic response of the materials, where  $R_1$  and  $R_2$  are the radius of the contacting bodies,  $E$  is the elastic modulus and  $\nu$  is Poisson's ratio. In the case of a flat substrate, one can assume  $R_2$  approaches infinity giving a very simple relationship between normal load and contact area. Hertz theory, although accurate at macroscopic levels, does not consider the effect of adhesive forces, which can become significant at nanoscales.

To address this, Johnson, Kendall, and Roberts (JKR)<sup>117</sup> developed a model accounting for the short-range adhesive forces within the contact region that predicted a larger contact area than Hertz. Also taking adhesion into consideration, Derjagin, Muller, and Toropov (DMT)<sup>118</sup> assumed that the deformed contact area does not deviate much from that derived from Hertz theory and incorporated the long-range adhesive force outside the contact region into their model. The difference between these two approaches (and the resultant contrasting predictions) was later reconciled by Tabor, who proposed that JKR and DMT are indeed two

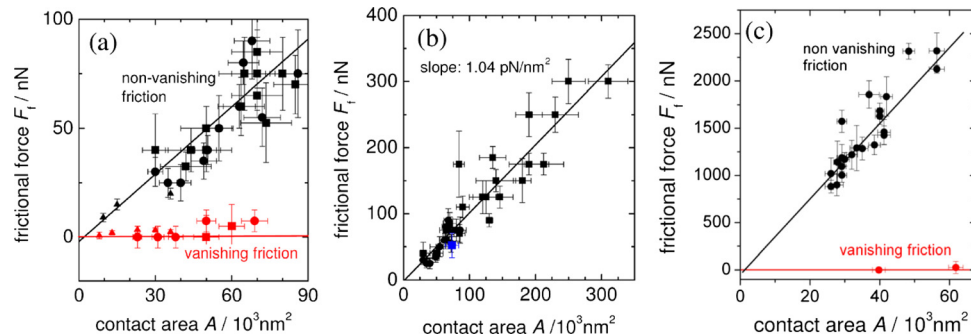


Fig. 8. (Color online) Experimental measurements the area-dependence of friction of sliding nanoparticles. Friction can increase with area as exhibited by the non-vanishing friction cases in (a), (b) and (c); friction can also be independent of contact area as exhibited by the vanishing friction cases in (a) and (c). Data in (a) and (b) from UHV measurements and data in (c) taken under ambient conditions. Lines are linear fits to the data (Ref. 115). Reprinted with permission from Dietzel *et al.*, Phys. Rev. Lett. **101**, 125505 (2008). © 2008 by the American Physical Society.

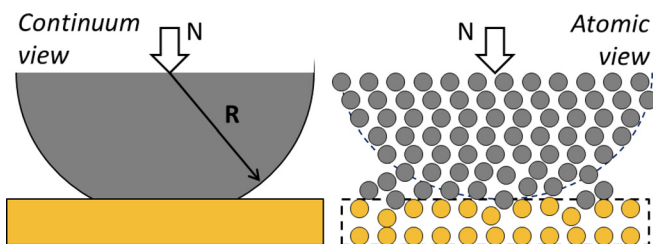


Fig. 9. (Color online) Schematic illustration of the continuum and atomic perspectives of the interface between an AFM tip and substrate.

extreme limits of the same theory: JKR is suitable for soft materials with strong adhesion, while DMT is more applicable to hard materials with low adhesion.<sup>119</sup> An analytical description of the intermediate regime was then formulated by Maugis with a Dugdale potential,<sup>120</sup> from which JKR and DMT models can be recovered in the limiting cases. The Maugis–Dugdale model has been widely utilized to interpret AFM measurement of atomic friction.<sup>121,122</sup> For a thorough summary of these methods, one can refer to Johnson's review paper.<sup>123</sup>

It is well known that continuum mechanics is valid when the dimensions of the studied object are much larger than the length scale of the discontinuity of the atoms. In an AFM, the size of the contact is on the order of nanometers, which is comparable to the length scale of atomic discontinuities. Therefore, despite the widespread use of continuum contact models, it is not certain that they can accurately describe single asperity contact. The contrast between continuum and atomistic views of contact is illustrated schematically in Fig. 9: Continuum mechanics assumes the tip and substrate are homogeneous elastic materials so that contact area can be determined from the geometry and elastic properties, while the atomic view takes individual atoms into consideration and the definition of contact becomes more complicated and depends on many more factors.

MD simulations have been used to show that, in some cases, continuum mechanics fails to capture the properties of nanoscale contacts. For example, Luan and Robbins revealed, for the same global geometry and loading conditions, contact area and stress can vary by two orders of magnitude due to atomic-level roughness.<sup>16,17</sup> This behavior cannot be captured by contact mechanics, which only takes the normal load and geometry into consideration. Therefore, other definitions of contact area have been suggested. One approach is to characterize contact using the distance between atoms in the tip and substrate. A distance is specified within which atoms are regarded to be in contact, then the area of the region circumscribing those atoms is taken as a measure of contact area.<sup>124,125</sup> The contact distance is usually prescribed based on the type of bonding expected to occur in the interface. This approach was applied in MD simulations of an H-terminated amorphous carbon tip sliding against an H-terminated diamond substrate,<sup>124</sup> which showed that, even at the nanoscale, the real contact area is characterized by roughness and is much smaller than the apparent contact area. Interestingly, it was also found that

the simulation data could be fit to the Maugis–Dugdale model. However, the success of the continuum model was attributed to its flexibility (three free fitting parameters), and not necessarily its ability to correctly describe the physical process taking place.<sup>124</sup> Although the definition of contact area in terms of atomic distance is more physically meaningful, it is currently limited by the fact that experimental validation at the atomic scale is currently not possible.

### C. Area dependence of friction

Despite the challenges with defining contact, many researchers have used both MD and AFM to study the effect of contact area on friction. These studies have shown that in some cases friction is proportional to the contact area,<sup>115,124,126</sup> while in other cases it is independent of contact area.<sup>115,127,128</sup> Figure 8 illustrates this duality clearly: Friction can increase with area as in the non-vanishing friction cases or friction can be independent of area as in the vanishing friction cases. One factor that could lead to this discrepancy is the effect of structural lubricity (introduced in a Sec. III C) where the stress inhomogeneity resulting from atomic structure in the buried interface can result in very low friction. In this case, friction does not necessarily scale with contact area as expected. Supporting this statement are observations of structural lubricity on graphite at both nano<sup>48</sup> and micro<sup>128</sup> scales. This, along with the contrasting area-dependence trends observed in AFM measurements, suggests that the atomic detail in the interface plays an important role. Specifically, if the interface is characterized by bond formation and rupture (e.g., covalent bonds in biochemical systems), or the contact is aligned, the friction may be significantly affected by the real contact area. However, if the interface is chemically passivated and the contact surface is misaligned, the contact area may have a limited effect on friction. Figure 10 demonstrates an MD prediction of friction between Pt(111)/Au(111) surfaces as a function of contact area at different orientation angles ranging from 0° aligned contact to 30° misaligned contact. Only the completely aligned case shows a linear relationship between friction and contact area; misalignment leads to a sublinear or negligible

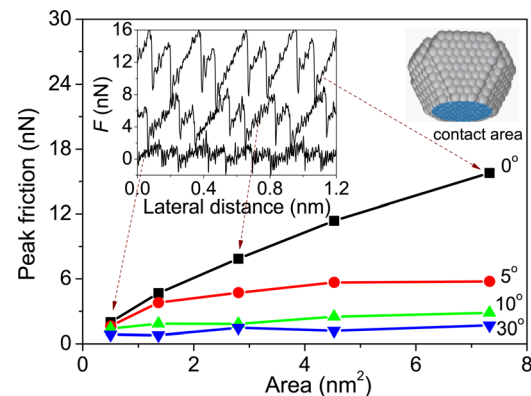


Fig. 10. (Color online) Friction as a function of contact area at different orientation angles between Pt(111)/Au(111) measured by MD simulation; 0° corresponds to perfectly aligned contact. Simulation parameters: EAM potential, load 0.6 nN, temperature 293 K, and speed 1 m/s.

effect. Note that, although misaligned contact is statistically more likely when two objects are brought together, local regions of aligned contact can arise through the occurrence of plastic deformation.

## D. Model considerations

To design an MD simulation consistent with experimental measurements, the model area should be prescribed to be the same as that in the experiment. Experimental contact area is typically estimated using continuum mechanics, despite questions about its accuracy at the nanoscale. Therefore, to design an MD simulation consistent with experimental measurements, the best approach is still to estimate the experimental contact area using the Maugis–Dugdale approach at a given normal load and then use that estimate to define the model contact size. This contact area can be prescribed exactly by creating a tip that is a truncated cone such as that in the inset of Fig. 10. With this approach, the degree of truncation can be specified such that the geometric contact area is exactly that estimated from AFM. Alternatively, many MD simulations model hemispherical tips based on the common assumption that the tip apex takes the shape of a sphere (supported by TEM images). In this case, the radius of model tip is chosen to match that of the AFM tip. While this approach can yield a more accurate representation of the global shape of the tip apex, it requires more computational capacity. In addition, after many cycles of sliding, an initially hemispherical AFM tip may become flattened due to wear.<sup>129</sup> Since MD simulation only captures the first few sliding cycles due to computational limitations, we cannot ensure the model-predicted evolution is the same as what occurs in an experiment.

## E. Summary and outlook

In summary, characterizing the effect of contact area on atomic friction is complicated by the fact that the definition of area is not explicit at atomic scales and that the area dependence of friction depends on other parameters such as commensurability. There are many opportunities for further research in this area. The first, and perhaps most important in terms of communication of new results, is defining contact area. As mentioned previously, there are multiple ways to define contact area and, even for a given definition, results can vary depending on the chosen parameters. A consistent definition would enable researchers studying different materials and using different methods to build on each others' results more efficiently.

Despite the progress that has been made in characterizing nanoscale contact area, we still fall back on continuum mechanics to make estimates from experimental data to design MD simulations. Introduction of an alternative would be a significant contribution to this field. More opportunities to improve contact characterization will likely come from *in situ* TEM, which, as discussed previously, can provide information about the geometry of the tip as it slides. Such information could be directly fed into an MD simulation such that the model tip apex is as similar as possible to that measured

in the TEM. Although matching tip shape cannot directly ensure that the contact areas are similar, this will be a major step forward in developing physically representative MD simulations.

## VI. LOAD

### A. Overview

A general and intuitive picture of sliding contact is that frictional resistance will increase with the normal load. As mentioned in the Introduction, this is described by the classical Amontons–Coulomb law,  $F = \mu N$ , which states that the friction force  $F$  is equal to a friction coefficient  $\mu$  times the normal load  $N$ . This expression works quite well on larger length scales. However, on the atomic scale, the role of adhesion becomes significant, and the relationship between normal load and friction may no longer be linear. Other factors, such as the evolution of the contact can further affect this relationship. In this section, we describe how atomic friction has been found to vary with load in AFM experiments and MD simulations and discuss the mechanisms underlying observed load-dependent variation. Then, we discuss guidelines for how to apply a normal load to a model tip and some considerations for using those simulations to study load-dependence.

### B. Load dependence

In classical contact mechanics, friction is related to normal load through the contact area. As load increases the contact area increases as described, for example, by the Hertz model in Eq. (5). If we assume a constant shear stress  $\tau$  in interface, friction is simply  $F = \tau A$ . If we further assume the effect of normal load on shear stress is negligible, then we can derive

$$F = \pi\tau \left( \frac{RN}{E^*} \right)^{2/3}. \quad (6)$$

However, this model assumes that the normal force is equal to the applied load which, for nanoscale contacts, may not be true due to the non-negligible role of adhesion. Contact area models that incorporate adhesion (e.g., DMT and JKR) were discussed in Sec. IV. Integrating those expressions into the relationship between force and area yields<sup>122</sup>

$$F = \pi\tau a_o \left( \frac{\beta + \sqrt{1 - N/N_o}}{1 + \beta} \right)^{4/3}, \quad (7)$$

where  $\beta$  is a transition parameter between 0 and 1 (when  $\beta = 1$ , it is the JKR model; and when  $\beta = 0$  it is the DMT model),  $a_o$  is the contact area when the applied load is zero, and  $N_o$  is the adhesion force. Regardless of the value of  $\beta$ , this expression predicts that friction increases sublinearly with load.

It is generally found from AFM measurements and MD simulations that friction increases with normal load. However, the exact nature of this increase is still

controversial: Friction has been reported to increase linearly with load,<sup>130,131</sup> increase with load faster than linearly,<sup>49</sup> and exhibit a sublinear dependence as predicted by Eq. (7).<sup>16,121,122,124,132</sup> Here we look at the problem from the perspective of atomic-level mechanisms and suggest that the effect of normal load on friction depends on both the chemical and mechanical properties of materials, and therefore may differ from case to case. For example, with chemically inert surfaces geometry, elastic deformation and surface roughness may be the main factors involved in load-dependence behavior. However, for chemically active surfaces, it may be the formation and rupture of bonds that predominantly determines friction. In addition, for metallic materials, junction formation and wear have to be considered. Hence, caution must be taken when attempting to describe atomic friction behaviors for different materials through a generalized equation.

Here we show an example in which wear and plastic deformation play a role in determining the effect of load on friction. This example demonstrates the diversity of the physical processes that occur during atomic friction and highlights the deficiency of continuum mechanics models. Figure 11 shows the load dependence of friction on a Au(111) surface measured by Gosvami *et al.*<sup>49</sup> As the normal load increases from  $-2$  to  $4$  nN, the friction varies little. After that, however, a transition occurs where there is a substantial increase of friction. It was suggested that the silicon AFM tip picked up gold atoms from the substrate so that there was a metal/metal interaction between the tip and substrate and a metallic junction formed when the tip was brought into contact.<sup>47,49</sup> In the low load regime, the metallic junction remains stable. Once the load exceeds a threshold value, this is no longer the case, which leads to the onset of wear and a significant increase of friction with normal load.

The mechanisms suggested above can be verified using MD simulation to “see” what is happening in the buried interface during sliding at different loads. Simulation-predicted load dependence from a simulation of Pt sliding a

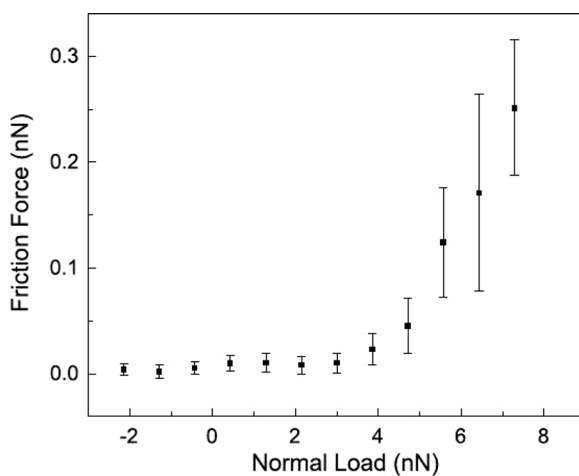


Fig. 11. AFM measurements of the load dependence of mean friction on a Au(111) surface in an ultra-high vacuum environment (Ref. 49). Reprinted with permission from Gosvami *et al.*, Tribol. Lett. **39**, 19 (2010), Fig. 4. © 2010 by Springer and Business Media.

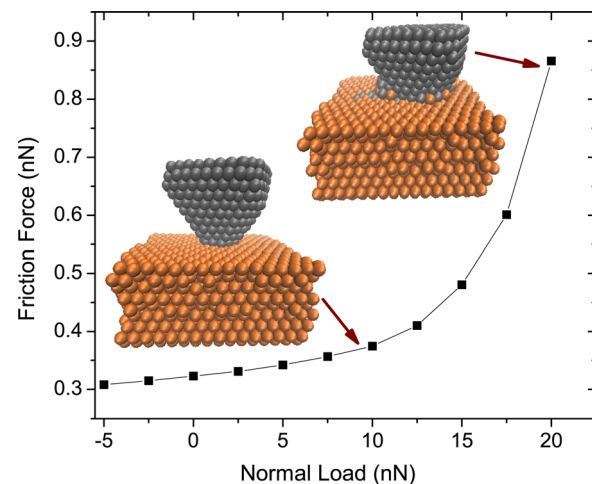


FIG. 12. (Color online) MD simulation of mean friction as a function of normal load for a Pt/Au(111) system. Inset are illustrations of atomic configurations during sliding at  $N = 10$  nN (left) and  $N = 17.5$  nN (right). Simulation parameters: EAM potential, temperature 10 K, speed 1 m/s, and contact area  $1.2 \text{ nm}^2$  ( $30^\circ$  misalignment angle).

Au(111) surface in misaligned contact is shown in Fig. 12. A stable truncated cone-shaped Pt tip is used to simulate the metallic junction formed between tip and substrate. Similar to the experimental result shown in Fig. 11, we observe a transition before which the friction increases very slowly with load. The simulation snapshots shown in the inset of Fig. 12 reveal that at low loads the tip and contact shape are constant while at high loads wear occurs in the buried interface through the transfer of atoms between tip and substrate. The atom transfer results in (a) a larger contact area and (b) rearrangement of atoms to more energetically favorable positions (aligned) positions. Since friction is higher in aligned contact as discussed in Sec. III, both of these effects increase friction. These behaviors cannot be described by traditional continuum mechanics theory of sliding friction, which do not account for the formation of a metallic junction or plastic deformation through rearranging of atoms. The same is true for other materials and conditions where effects not described by continuum mechanics play a role.

### C. Model considerations

Next we look at how to apply a normal load in MD simulation. AFM measurements of atomic friction are usually conducted in contact mode, where the tip is brought in very close proximity to the substrate, and an instantaneous feedback system helps keep the normal load applied to the tip constant. To capture this in an MD simulation, a constant normal force can be directly applied to the atoms in the uppermost layers of a model tip. As mentioned in Sec. IV, often these layers are treated as a rigid body. In some simulations reported in literature, the normal load is applied by enforcing a constant distance between the tip and substrate. However, this can be problematic for two reasons. First, normal load is not in fact constant at a constant distance because of peaks and valleys in the energy landscape due to the discreteness of the atoms. Second, preventing the tip from

moving in the normal direction can artificially hinder the occurrence of wear or plastic deformation, which is very common and sometimes the dominant effect in experimental measurements. Although controlled distance can be easier to implement in MD simulation, we strongly recommend applying a constant force to physically represent the AFM measurement.

#### D. Summary and outlook

In summary, to this point, a clear picture of how load affects atomic friction has not been achieved because different materials and environments can give rise to distinct physical processes, which directly affect load-dependence. However, since experiments on a variety of materials and under different conditions are now available, modelers have the opportunity to distil these varied results into a more general picture. The power of an MD simulation is that we can systematically investigate the effect of individual parameters, which is not possible in an experiment; for example, contact area and load can be separated from one another in a simulation, but are necessarily related in an experiment. This type of systematic analysis of the effect of load could lead to general guidelines that would be similar to Amontons–Coulomb law in that they can be applied to any system, but would be more complex because they would require more variables to incorporate the various other effects described in this section.

## VII. TEMPERATURE

### A. Overview

Temperature, a reflection of the thermal kinetic energy of constituent atoms, plays an essential role in atomic friction. Recent advancements in AFM capabilities have enabled friction measurements over wide temperature ranges, from cryogenic conditions to a few hundred Kelvin. These new experiments have revealed several interesting trends. The

most widely recognized trend is that friction decreases with temperature.<sup>40,133,134</sup> For example, Fig. 13 (Ref. 134) shows that friction decreases as temperature increases from 109 to 295 K. In addition, a few recent measurements have shown that atomic friction exhibits a peak or plateau at low temperatures (around 50–200 K) beyond which friction decreases with temperature.<sup>135–138</sup> Both the low temperature peak/plateau and the general trend of decreasing friction with increasing temperature have been measured on a variety of materials including silicon, SiC wafers, ionic crystals, and graphite.

In MD simulation, one can easily control the temperature and therefore simulations are ideal tools with which to study how friction varies over large temperature ranges without the complexity associated with experiments at very high and very low temperatures. MD-based temperature dependence studies have been performed on a variety of substrate materials including metals (Cu and Au), diamond, and alkylsilane monolayers.<sup>37,40,56,111,139</sup> All previous MD studies have reported a decrease of friction with temperature.

### B. Mechanisms of temperature dependence

Bearing the above-mentioned temperature dependence trends in mind, we now look at the proposed underlying mechanisms. Decreasing friction with increasing temperature is popularly believed to be due to thermal activation: Higher temperatures provide more thermal energy, which helps the tip creep over energy barriers sooner leading to lower friction. This concept can be analyzed using the Prandtl–Tomlinson (PT) model<sup>140,141</sup> to describe the energetic evolution of the system and transition state theory<sup>142</sup> to describe the effect of thermal activation. In the framework of the PT model, the tip is viewed as a single atom ball dragged by a harmonic spring over a sinusoidal corrugation potential which represents the interaction with the substrate as shown in Fig. 14. Then, the total potential energy of the system can be formulated as

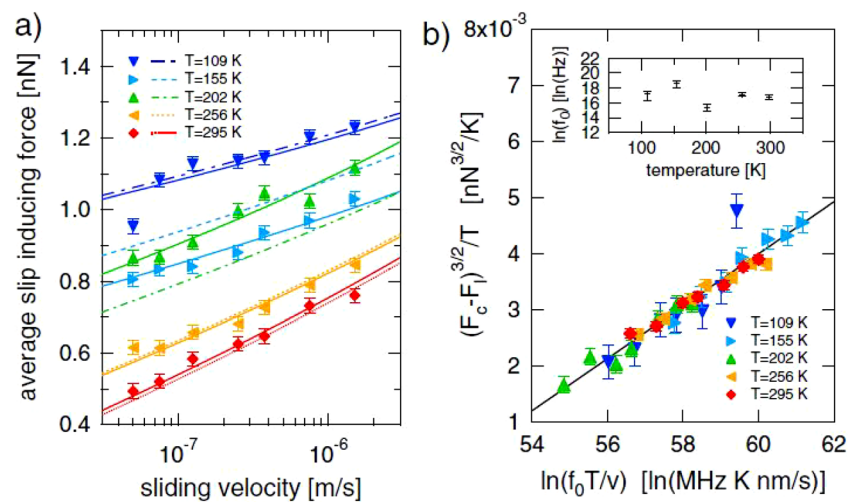


Fig. 13. (Color online) (a) AFM measurement of the slip-inducing forces (maximum friction) as a function of sliding velocity at different temperatures. (b) All experimental data at different temperatures and velocities fall onto the same curve predicted by the thermal activation theory given in Eq. (10). The inset shows a plot of the attempt frequency as a function of temperature (Ref. 134). Reprinted with permission from Jansen *et al.*, Phys. Rev. Lett. **104**, 256101 (2010). © 2010 by American Physical Society.

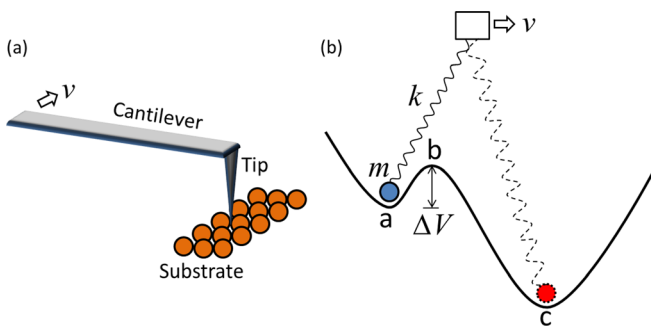


FIG. 14. (Color online) Illustrations of (a) an AFM cantilever pulling the tip to slide over a substrate and (b) the corresponding PT model in which the AFM system is reduced to a mass-spring system. In the PT model, the model tip is confined within the potential well and hops over the energy barrier with the assistance of thermal activation.

$$V(x, t) = -\frac{U}{2} \cos\left(\frac{2\pi x}{a}\right) + \frac{1}{2}k(vt - x)^2. \quad (8)$$

The first term on the right hand side of this expression describes the corrugation potential where  $U$  is the amplitude,  $x$  is the tip displacement, and  $a$  is the lattice spacing of the substrate. The second term is the elastic potential resulting from the interaction between the tip and support where  $k$  is the spring stiffness,  $t$  is time, and  $v$  is the sliding speed of the support. The total energy evolves when the driving support moves forward at constant velocity, denoted by the  $vt$  term. In the absence of temperature, the slip occurs only when the energy barrier,  $\Delta V$  in Fig. 14(b), disappears completely. With the assistance of thermal activation, the tip can creep over the energy barrier from potential well  $a$  to  $c$  earlier, which means it requires a smaller force (friction) to move the tip forward. The creep due to thermal activation can be described by Transition State Theory (TST) in the harmonic approximation such that the transition rate from potential  $a$  to  $c$  is given by

$$\kappa = f_o \exp\left(-\frac{\Delta V}{k_B T}\right), \quad (9)$$

where  $f_o$  is the attempt frequency of the system, which is a reflection of the characteristic frequency of the tip confined in a potential energy well,  $\Delta V$  is the energy barrier,  $k_B$  is the Boltzmann constant, and  $T$  is the temperature. Combining Eqs. (8) and (9), the relation between friction and temperature (and sliding velocity) can be derived<sup>42,88,143</sup>

$$F = F_c - \left| \beta k_B T \ln\left(\frac{v_c}{v}\right) \right|^{2/3}, \quad (10)$$

where  $F_c$  is the maximum friction at  $T=0$ ,  $v_c = \frac{2f_o\beta k_B T}{3k_{\text{eff}}\sqrt{F_c}}$  is the critical velocity,  $k_{\text{eff}}$  is the effective stiffness (see Sec. IV), and  $\beta$  is a parameter determined by the shape of the corrugation potential. In the derivation of Eq. (10), it has been assumed that the transition point (the position of the tip when it slips forward) is very close to the critical point (point  $b$  in Fig. 14) and that the attempt frequency  $f_o$  is constant. Both of these assumptions are not strictly true however and closer scrutiny of the form of  $\beta$  and the variation of  $f_o$  can be

found in Refs. 144 and 145. The concept of thermal activation and the corresponding mathematical formulation have been used to interpret many experimental measurements of temperature and velocity dependence of friction.<sup>2,40,42,88,133,134</sup> Experimental friction versus temperature data fit to thermal activation theory is shown in Fig. 13.<sup>134</sup>

In addition to thermal activation, other mechanisms have been proposed to account for the different trends observed in AFM measurements. For example, the friction peak arising in the low temperature regime (around 50–200 K)<sup>135–138</sup> is not captured by thermal activation theory. To address this issue, it has been suggested that thermal activation not only assists in the rupture of bonds, but also in the formation of bonds; the competition between the two leads to the friction peak at low temperature.<sup>137,146</sup> The concept of bond formation and rupture seems promising but is still at a phenomenological stage. Atomic-scale verification of this concept, which might be available from an MD simulation with an appropriate interatomic potential, could provide more insight. It has also been proposed recently that athermal noise<sup>147,148</sup> such as mechanical vibration, acoustic noise, and electromagnetic interference inherent in the AFM system might assist the tip to hop over energy barriers, and hence cause a suppression of friction at low temperatures.<sup>149</sup> Unfortunately, this cannot be verified using MD simulation so far because noise inherent in an AFM measurement is not localized at the tip apex and contact, which are only aspects of the system explicitly described by traditional MD simulation.

### C. Model considerations

Having discussed possible mechanisms related to the effect of temperature on atomic friction, we now focus on how to control temperature in an MD simulation. First, consider how energy is dissipated in a realistic friction system. The general picture is that, when sliding occurs (especially the unstable slip phase during stick-slip motion), the mechanical energy will generate phonons, excite electrons from one band to another, or excite electron-hole pairs in the tip and substrate. The localized energy then propagates away through phonon transport or electron conductivity and ultimately dissipates as thermal energy to the whole system. Due to the size limitations of MD simulation, the model describes large systems in an effective way using numerical boundary conditions. In this case, the energy generated cannot propagate far away, instead it is reflected at a fixed boundary or re-enters the domain at a periodic boundary, either of which leads to an unphysical accumulation of heat. In addition, since electrons are not explicitly modeled in an MD simulation, that dissipation channel is not available to the model system. To address these issues, a numerical thermostat is often applied in the simulation to cool down the system.

Many different thermostat schemes have been developed. The simplest approach is to rescale the velocity of atoms to obtain the desired temperature. However, there are significant issues with this approach since it does not generate

samples from the canonical ensemble and the rate of heat removal is disconnected from system properties. These issues limit the usefulness of velocity rescaling in practice and have led to the development of more sophisticated methods. Currently, the most widely used techniques are the Langevin thermostat, in which a random force associated with the target temperature is added to the dynamics of atoms, and the Nosé–Hoover thermostat, in which a new degree of freedom is introduced to simulate the interaction between the atoms and a thermal bath; a more comprehensive discussion of these methods in the context of friction modeling is available in Ref. 150.

In simulations of atomic friction, if no thermostat is applied, a lateral sliding will lead to an increased rate of energy generation and corresponding temperature rise. A properly implemented thermostat will extract the energy generated such that the system temperature fluctuates about the target value. Figure 15(a) shows the temperature of a system subject to a constant sliding speed with and without a Nosé–Hoover thermostat at 300 K. Typically, in simulations of atomic friction, the thermostat is applied only to the atoms away from the contact region so that the heat generated during sliding can be effectively dissipated, but the dynamics of the contacting atoms is not altered in the process.<sup>150</sup> The thermostat is applied to atoms that are at least several atomic layers from the contact in both tip and substrate while the interface atoms (the most bottom few layers of the tip and the most top few layers of the substrate) evolve based on Newtonian dynamics. This targeted thermostat approach is illustrated in the inset of Fig. 15(b): In practice, depending on the geometry, interatomic potential and speed/load conditions, the simulation-predicted friction may be the same regardless of where the thermostat is applied. However, the more physically realistic approach is to minimize the impact the numerical thermostat might have on the dynamics of the system by applying it away from the contact. An example of MD-predicted friction variation with temperature obtained using this approach is shown in Fig. 15(b). Consistent with thermal activation theory, the friction decreases with increasing temperature.

#### D. Summary and outlook

The temperature dependence of atomic friction is complex and depends to some degree on the materials and conditions of the experiment. The most commonly observed trend, that friction decreases with temperature, can be described by thermal activation theory. Since MD simulations necessarily include thermal noise, they are able to predict the associated decreasing friction with temperature. However, there are other observations, such as a friction peak or plateau at low temperatures, which cannot be explained by thermal activation. Possible mechanisms include the bond rupture and formation due to thermal activation, wear, and athermal noise. These trends have not, to this point, been captured by MD simulations, and therefore, the proposed mechanisms have not yet been validated at an atomic scale. However, simulations could in fact capture some of the processes (such as bond formation/rupture or wear) on which these theories are

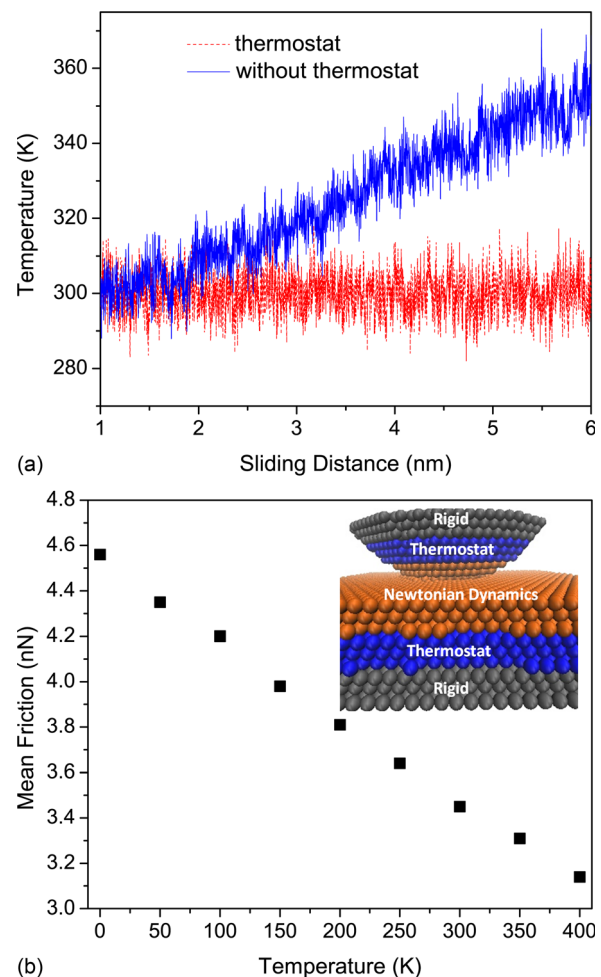


FIG. 15. (Color online) (a) Temperature of the contact interface varying with sliding distance from an MD simulation with Pt(tip)/Au(substrate) system. The initial temperature of the simulation is 300 K. Once sliding begins, the average temperature increases with distance if there is no thermostat to remove thermal energy from the system (solid line) but fluctuates about the prescribed temperature if the Nosé–Hoover thermostat is applied (dashed line). (b) Mean friction as a function of temperature from an MD simulation of atomic friction between a Pt(tip) and Au(substrate). Inset is a schematic illustrating a thermostat being applied to atoms away from the contact in a simulation of atomic friction. Simulation parameters: EAM potential, load 0 nN, speed 2 m/s, and contact area  $1.3 \text{ nm}^2$  (aligned).

based. Finding ways to introduce other possible effects into an MD simulation can provide an excellent opportunity for models to validate proposed theories and help explain experimentally observed trends.

As mentioned previously, there are multiple energy dissipation channels available to an AFM system (phonon, electrical excitation, or electron-hole pair excitation) while MD can only capture phonon vibration. The impact of this limitation cannot be estimated since we do not know how significant each dissipation channel is for frictional systems in general. However, a sudden drop of friction was observed when the temperature decreased across the critical temperature of 9.2 K for superconductivity of Niobium films.<sup>151</sup> This implies that decreasing the temperature can close the electrical excitation energy dissipation channel and therefore that electrical dissipation is an important channel for atomic

friction for these films.<sup>151</sup> These results encourage additional investigation of energy dissipation channels and their temperature-dependent role in friction.

There are opportunities for continued research into how to apply a physically realistic thermostating scheme. For example, all thermostats require that one or more parameters be specified that determine how fast energy is removed from the system. It was reported that, for the Langevin thermostat, there exists an optimal viscous damping, with which results are indistinguishable from the exact solution. The optimal value is simply the one that maximizes dissipation.<sup>152</sup> Unfortunately, a general guideline for choosing these parameters is not available and often researchers rely on trial and error to identify optimal values. Understanding the effect of thermostats on sliding friction at the nanoscale is still an ongoing research area<sup>152,153</sup> and one that has the potential to improve the predictive ability of atomic friction simulations.

Lastly, it is important to point out that controlling the system temperature at some fixed value may not in fact be physically realistic. Specifically, local heating at the interface is typical in most sliding contacts. Therefore, modeling sliding might be best done by allowing the temperature rise; the challenge lies in determining how much. Unfortunately, such information is not typically available from an experimental measurement as it would require *in situ* contact area temperature measurements. However, given the important role temperature plays in atomic friction, there is significant potential for development of new methods that can be used to determine and accurately capture thermal effects in a simulation.

## VIII. VELOCITY

### A. Overview

The Amontons–Coulomb law states that the macroscopic friction is independent of sliding velocity. This is not necessarily the case at the nanoscale: AFM measurements of atomic friction on a variety of different materials have shown velocity plays an important role. The dependence of friction on velocity can be explained by the thermal activation mechanism presented in Sec. VII. This theory predicts that larger sliding speeds correspond to less time for thermal motion to help the tip to hop out from its current low energy state. The result is that atomic friction logarithmically increases with sliding velocity.<sup>2,42,47,88,154</sup> Figure 13 shows an example of an experimentally observed logarithmic increase of friction with speed where the data are fit to thermal activation theory. This trend is observed in most cases for moderate sliding speeds. However, when the velocity is too large [larger than the critical velocity  $v_c$  in Eq. (10)], there is little contribution from thermally-activated hopping and the friction saturates at its maximum value. Aside from thermal activation, other mechanisms that could cause observed velocity dependence have been proposed. For example, Chen *et al.*<sup>155</sup> found that the logarithmic increase can be changed to a logarithmic decrease when the sliding surface is terminated by groups such as –OH, –COOH,

and –NH<sub>2</sub>, which allows the formation of H-bond networks within the terminated surface. It has also been argued that a smaller velocity will allow more time for bonds to form between the tip and substrate, which will then lead to larger friction.<sup>137,138,146</sup> Lastly, the formation of a meniscus in humid environments can affect velocity dependence.<sup>133,156,157</sup>

The velocity dependence of friction can be studied using MD by simply varying the speed at which the model tip apex moves. The driving velocity is either applied directly to the topmost atoms in the tip or to the virtual atoms which pull the tip through a harmonic spring if compliance is considered. However, using MD simulation to investigate velocity dependence under AFM conditions remains a challenge because of the timescale limitations of the simulation. A typical velocity accessible to AFM to obtain atomically resolved stick-slip event is in the range of nm/s to μm/s. With techniques designed specifically for measuring friction, maximum sliding speeds can reach mm/s (Refs. 158 and 159) but only by sacrificing the resolution needed to observe stick-slip. Most AFM friction studies are reported at slower speeds. On the other hand, most MD-based atomic friction studies are performed at speeds on the order of m/s. The factor that restricts simulations to fast speeds is the simulation time step which, in order to capture the characteristic dynamics of individual atoms, is typically around 1 fs. The small time step limits the maximum duration of the simulation to ns. This means that model sliding speeds must be on the order of m/s to capture a sufficiently long sliding distances to observe multiple periods of stick-slip. Therefore, most simulations are performed at much faster speeds than the corresponding experiments and model predictions of velocity dependence must be extrapolated to the experimental speed regime. Such extrapolation can be inaccurate because the effect of velocity may be different in different velocity regimes. For example, it has been shown theoretically and using MD simulation that athermal effects can play an important role at high velocities such that the logarithmic dependence is not observed at those speeds.<sup>2,160</sup> The velocity discrepancy and associated differences in the underlying mechanisms reduce the effectiveness of MD as a means of interpreting AFM experiments.

To bridge the speed gap, several techniques have been developed to accelerate simulations. The techniques we will focus on here are those designed to take advantage of the timescale gaps that exist in so-called rare or infrequent event systems. An event can be described as infrequent if (a) the time between events is much longer than the duration of the event itself, and (b) any new event is uncorrelated with events prior to it. Atomic stick-slip friction meets this criterion since slips are rapidly occurring events separated by long durations of stick. Here we will discuss three types of accelerated methods for infrequent event systems: hyperdynamics,<sup>161</sup> temperature accelerated dynamics,<sup>162</sup> and parallel replica dynamics.<sup>163</sup> We will first present all three methods for a general case, then we will illustrate the application of one of the techniques, parallel replica dynamics, to study velocity dependence in atomic-scale friction.

## B. Accelerated MD methods

To present the theory underlying accelerated methods, we use the reduced-order system shown in Fig. 16. Initially, the system resides at the potential well *a* and experiences thermal vibration with a characteristic time  $\tau_t$ . The transition from potential well *a* to *c* occurs on the time scale  $\tau_e$ . If  $\tau_e \gg \tau_t$ , then we claim that the transition is an infrequent event and can be described by TST. Within this theory, the transition rate from one potential well to another is described by Eq. (9). The techniques to accelerate MD simulation that we will discuss are designed to increase the transition rate in different ways. At a high level, the three techniques accelerate transitions by decreasing the depth of the potential energy well (hyperdynamics), increasing the temperature (temperature accelerated dynamics), and parallelizing the system in time (parallel replica dynamics).

Hyperdynamics<sup>161</sup> is based on modification of the original potential energy surface to accelerate the occurrence of transitions by adding a positive potential bias  $\delta V(r)$  as shown in Fig. 16(a), where  $r$  is the configuration space. Without modification, the transition rate is described by Eq. (9). Adding the potential bias, the transition rate increases by a factor of  $\langle \exp[\frac{\delta V(r)}{k_b T}] \rangle$  where  $\langle \rangle$  indicates an ensemble average; this increase is called a boost factor. The advantage of hyperdynamics comes from the magnitude of the boosting factor, i.e., the potential bias is magnified by an exponential term, such that a substantial acceleration can be achieved. Hyperdynamics has been applied to simulations of atomic stick-slip friction by Kim *et al.*<sup>110</sup> who achieved sliding velocities comparable to experiment. However, it is worth pointing out that hyperdynamics relies on identifying an effective potential bias.<sup>161,164</sup> The construction of a potential bias that guarantees the transition regions are not influenced and the process still occurs via rare events is often time-

consuming.<sup>165</sup> An interface with too many atoms in the contact or where the friction process is dominated by wear can introduce additional challenges. Lastly, and very relevant to atomic friction, this method does not ensure that correlated events are captured properly, which means that it may not be able to predict multiple slips (slip over more than one energy barrier).

Temperature-accelerated dynamics<sup>162</sup> speeds up transitions by increasing the temperature of the system. Its boost factor at some high temperature  $T_{\text{high}}$  can be easily obtained from Eq. (9) as  $\exp[\Delta V(\frac{1}{k_b T} - \frac{1}{k_b T_{\text{high}}})]$ . Temperature-accelerated dynamics has the potential to achieve the largest boost factor of the three approaches discussed here. However, this method is based on a more strict assumption, i.e., the system must obey the harmonic TST approximation, which may not necessarily be the case for all infrequent event systems. In addition, for atomic friction, high temperature could cause the onset or suppression of wear, chemical reactions, or other processes.<sup>30,136</sup> These may be the reason that, to our best knowledge, there is no study utilizing temperature-accelerated dynamics to slow down the sliding speed of atomic friction simulations.

The parallel replica dynamics (ParRep) method uses multiple replicas  $M$  of the original system to increase the transition rate. Note that this is distinctly different from typical MD parallelization in which the simulation cell is divided into many different spatial domains and each processor handles integration of the equations of motion for atoms in a given domain. In contrast, ParRep employs temporal parallelization where all replicas perform integration for the entire simulation cell but the simulation time is distributed among them. All  $M$  replicas share the same potential energy surface but with different initial velocities such that all the replicas evolve along different paths and the transition rate can be accelerated by a factor of up to  $M$ . This method has the advantage that it does not require modification of the potential energy surface or temperature of the system. However, its boost factor depends on the number of processors available to researchers, so a large-scale high performing cluster is needed for a substantial acceleration. This method has been recently used to accelerate MD simulation of atomic friction and significantly reduce the sliding speed.<sup>2,166–168</sup>

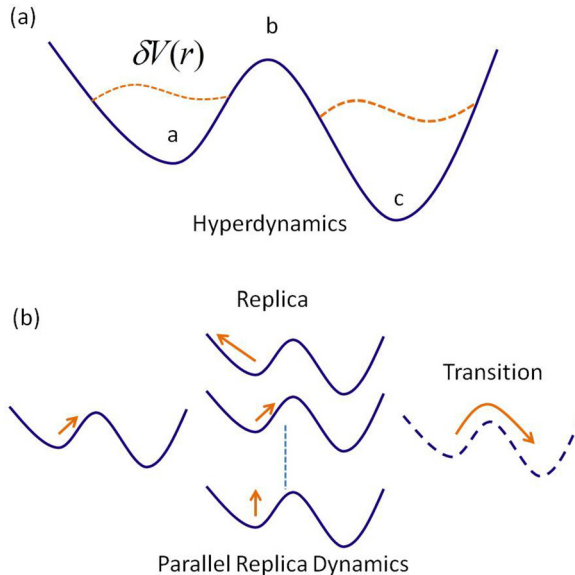


Fig. 16. (Color online) Schematic of a reduced-order system. (a) In hyperdynamics the potential is modified by adding a positive bias  $\delta V(r)$  to increase the transition rate. (b) Schematic of parallel replica dynamics. The original system is replicated to help find the transition path.

## C. Parallel replica dynamics of atomic friction

Atomic stick-slip friction is a typical infrequent event where stick occupies most of the time, and slip occurs infrequently. This meets the fundamental criteria necessary for the application of ParRep. However, atomic friction has a feature that is not accounted for in the original ParRep theory and adds complexity to its implementation, i.e., atomic friction is a driven process in which the potential energy surface evolves with time as the tip is pulled by the cantilever. Indeed, external driving arises in many physical processes, for example, tensile or shear loading. To enable the method to be used for such systems, Uberuaga *et al.* extended ParRep to driven systems and provided a rigorous mathematical proof of its accuracy.<sup>169</sup> The basic idea is that

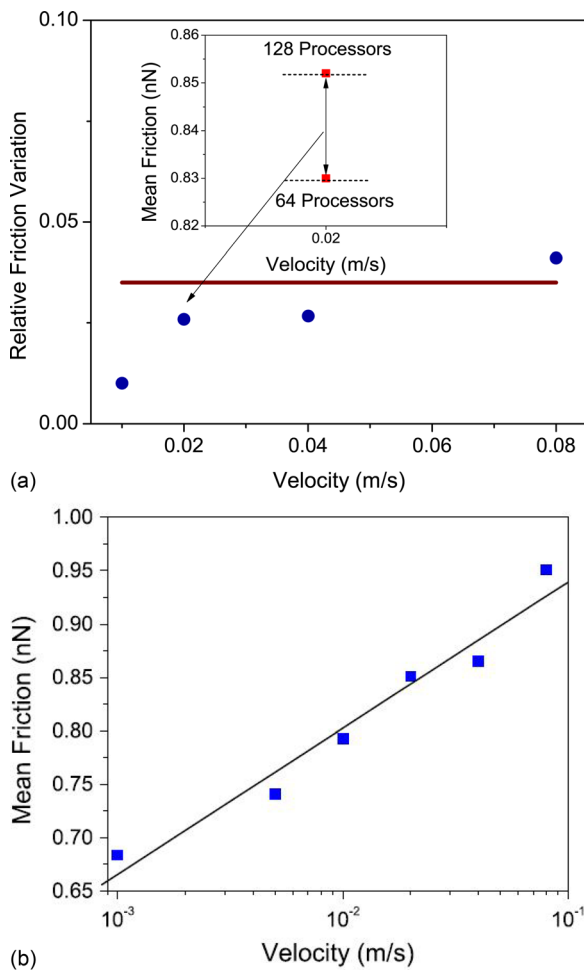


FIG. 17. (Color online) (a) Relative friction variation (variation divided by mean friction) predicted using parallel replica dynamics when run on 128 replicas vs 64 replicas (circles and insets) and the expected relative variation due to MD simulation noise (solid line). (b) Mean friction as a function of sliding velocity measured between Cu(111)/Cu(111) interface: squares represent ParRep simulation and the solid line is a logarithmic fit to that data. Simulation parameters: EAM potential, load 0 nN, temperature 300 K, and contact area 1.3 nm<sup>2</sup> (aligned) (Ref. 167). Reprinted with permission from Martini *et al.*, Tribol. Lett. **36**, 63 (2009), Fig. 5. © 2009 by Springer + Business Media.

if we drive the system on each replica with a rate  $R_r$ , and we have  $M$  replicas in total, theoretically we can achieve a driving rate of  $R = R_r/M$ . The derivation is based on an assumption, that the transition rate at any given time is determined only by the boundary conditions, not of the driving rate. In other words, we need to guarantee that the driving rate on each replica is small enough that the system is in a quasi-static state.

For atomic stick-slip friction, this means that the sliding velocity on each replica must be small enough that thermal activation is still the dominant factor assisting the tip to hop out of its current low energy state. To determine how slow is slow enough, we can analyze the variation of friction predicted by the simulation with different number of replicas. If the system is indeed quasi-static, the replica-dependence will be minimal (less than the noise associated with the stochastic nature of MD). As an example, Fig. 17(a) shows the

variation of mean friction between Cu(111)/Cu(111) surfaces calculated by ParRep using different number of processors. For this system, the replica-induced variation is less than the noise level when the sliding speed is below about 0.04 m/s.<sup>167</sup> Since ParRep is being implemented specifically to model slow speeds, the error that arises at fast speeds is acceptable. However, it is important to perform this type of analysis for each system studied to determine the maximum speed that the method should be applied. To illustrate the power of the ParRep method for modeling atomic stick-slip friction, a representative plot of velocity dependence from the Cu(111)/Cu(111) system is shown in Fig. 17(b).<sup>167</sup> In this case, with the help of ParRep, sliding speeds as low as 10<sup>-3</sup> m/s were obtained. Further, a logarithmic fit to  $F(V)$  is obtained consistent with thermal activation theory.

#### D. Summary and outlook

In summary, atomic friction generally increases with sliding speed in both MD simulations and AFM experiments. However, the experiments cannot be used to directly validate the simulations because of the significant time-scale gap between the two techniques. This gap limits the extent to which the simulations can be used to explain mechanisms underlying experimentally observed trends. To address this issue, there are methods available through which the sliding speeds can be decreased by accelerating the simulation. One such method, which has been shown to be effective for atomic friction is parallel replica dynamics. An effort to bridge the gap between AFM experiment and MD simulation is shown in Fig. 18, in which the velocity in simulation has been decreased to 0.005 m/s using ParRep.<sup>2</sup> It is notable that, despite the use of the accelerated method, there is still a three orders of magnitude difference between simulation and experimental speeds. Accelerated MD is still an ongoing

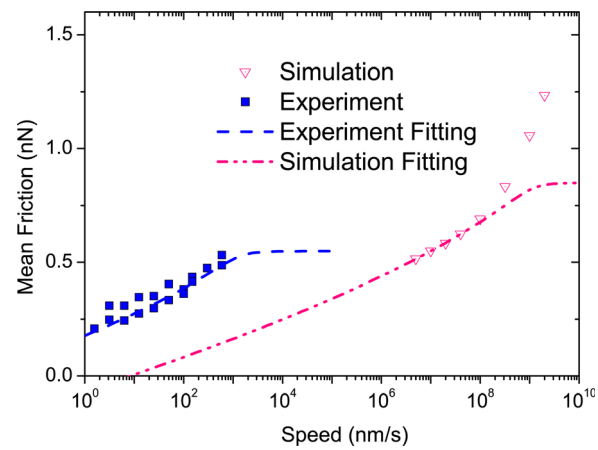


FIG. 18. (Color online) Mean friction measured by AFM (squares) for speeds between 1 and 1000 nm/s, and predicted via ParRep MD simulation (triangles) for speeds between 0.005 m/s and 2 m/s between Pt/Au(111). The dashed curve and dotted curve are fitted using the thermal activation model [Eq. (10)] for experimental and simulation data, respectively. All other parameters from materials, orientation, effective stiffness, contact area, normal load and temperature between AFM and MD are optimally matched based on the methods introduced in previous sections (Ref. 170). Reprinted with permission from Dong *et al.*, Tribol. Lub. Tech. Feb. 17 (2012). © 2012 by Society of Tribologists and Lubrication Engineers.

research area,<sup>165,171</sup> and we anticipate that as these numerical techniques develop and faster computations resources become available, slower and slower model sliding speeds will be accessible to the simulations. Slower speeds may also be accessible by optimizing implementation parameters (e.g., duration between transition checks in ParRep) and combining multiple accelerated methods. The ultimate goal is to measure/predict friction with experiments/simulations at the same sliding speed.

## IX. CONCLUSION

Over the course of this review, we have demonstrated that materials, surfaces, compliance, contact area, load, temperature, and velocity can all affect atomic friction significantly. More importantly, we have shown that, to make quantitative comparisons between MD simulation and AFM experiment, each of these effects must be considered and introduced into a model carefully. Finally, for each parameter, we discussed the state of current modeling efforts and potential areas for future research that could be of great benefit to the field of nanotribology. We will now reiterate those opportunities in a more general sense.

One of the most significant limitations for MD simulation of any time-dependent process is the short time scale associated with the simulation. Due to the limitations of current computing power, the simulated duration is usually less than a microsecond. A direct consequence is the sliding velocity accessible to standard MD is on the order of 1 m/s, which is orders of magnitude faster than an AFM experiment. This not only precludes direct validation of simulations using experimental data, but restricts MD from contributing to our understanding of phenomenon associated with atomic friction that only emerges at long time scales. For example, friction ageing which describes the observation that static friction logarithmically increases with time on the order of seconds;<sup>172</sup> or the finding that static and sliding friction at the nanoscale can be differentiated only when the contact is in position for more than 25 ms.<sup>173</sup> To completely bridge the velocity gap, significant efforts are needed both to increase AFM scanning speeds and decrease the scanning speed in simulations. Further enhancement of the accelerated MD methods described in Sec. VIII is one approach that can be pursued from the simulation perspective. However, we encourage development of new and creative ways of addressing this important issue.

Similar to time-scale, the size-scale issue also limits the usefulness of MD simulation. As discussed previously, the model only explicitly captures the atoms at the apex of a very sharp AFM tip. This has several adverse affects as mentioned in Secs. III, IV and VIII. For example, MD simulation fails to capture the inertia of the massive microcantilever and its effect on speed dependence.<sup>2</sup> Also, the simulation cannot resolve the stiffness contributions of the main body of the tip and the cantilever, which are believed to have an important role in jump dynamics of the tip apex.<sup>45</sup> As computational hardware continues to improve, atomistic simulations will be able to increase in size. However, the gap

between a fully atomistic model of a sharp tip apex and an AFM tip can be expected to be significant in the foreseeable future. Two reasonable means of addressing this gap are through the use of multiscale methods or reduced order modeling. Another approach we expect to be extremely valuable as this field moves forward is use of MD simulation to obtain energetic information in conjunction with other techniques such as transition rate theory<sup>174</sup> and Monte Carlo methods<sup>144,175</sup> to shorten the simulation time.

Another aspect of MD simulations that provides opportunities for future research is the empirical potential. As discussed in Sec. II, the reliability of MD simulation depends primarily on the accuracy of the potential. Therefore, the importance of developing empirical potentials focusing on surface energy and mechanical properties cannot be overemphasized for atomic friction simulations. In addition, the range and variety of different materials that can now be measured means that more flexible and widely applicable potentials must be developed to complement new experimental discoveries. For example, the possibility of controlling friction by chemically modifying the substrate surface has recently been explored.<sup>176,177</sup> Complementing this type of experiment with an MD simulation will require a valid potential that captures the chemical bonds between heterogeneous atoms. In fact, as discussed in Sec. VI in terms of load-dependence, any model of structural or chemical evolution (i.e., wear) will require an empirical potential flexible enough to capture those changes. In addition, empirical potentials explicitly consider only the interaction between atomic nuclei, while in most cases the electrons and their associated effects are implicitly incorporated. As a result, MD simulation is suitable for the study of phononic friction, which is a reflection of the motion between atomic nuclei, but cannot capture electrical friction, which is related to the excitation of electrons. The introduction of quantum mechanics theory may enrich our understanding of these topics. Finally, while more and better empirical potentials are being developed, density functional theory (DFT) calculations can provide another avenue for researchers in atomic friction.<sup>177–182</sup> We expect that use of DFT for friction studies will increase in popularity both as a means of providing reference data to fit empirical potentials and to explore frictional mechanisms on their own.

Lastly, MD simulation that is intended to complement experiments requires feedback from the experiment to validate its accuracy. The potential for using *in situ* TEM to guide simulation design was mentioned in Secs. IV and V. Further development of experimental characterization techniques, such as APT, can provide more and different information about the interface during and after sliding. It is important to note that many new potentially useful technologies will not be specifically developed for tribology, or even for interfaces. We therefore encourage modelers to keep abreast of the latest experimental advancements and explore ways to take advantage of the data available through those advancements to improve model accuracy.

In summary, atomic-friction is a complex, yet fascinating phenomenon that has the potential to yield a great deal of

insight into frictional sliding on any length scale. As has been shown in this review, atomic friction is affected by many different interrelated properties of the contacting materials, as well as environmental and operating conditions. Atomistic simulation can help us understand these effects because it provides an atom-by-atom view of how the contact interface evolves and therefore the source of the resistance to sliding. However, to reach their full potential, such simulations must be developed in conjunction with experimental AFM measurements which provide validation and a reference for model design. Designing simulations that match the experiments as closely as possible is critically important to moving forward with atomic-scale friction research. We believe that understanding all of the factors that affect atomic friction is the first step towards being able to create a physically-realistic model. The goal of this review was to communicate what is currently known about these effects and the best practices for implementing them in a simulation. We hope that this serves as a foundation for researchers to explore new ideas and make profound breakthroughs in the area of atomic-scale friction.

## ACKNOWLEDGMENTS

Y.D. and A.M. would like to thank the U.S. National Science Foundation (CMMI 1068552) and the Air Force Office of Scientific Research (FA9550-12-1-0221) for support of this research. Q.L. thanks the support from the National Natural Science Foundation of China (11272177), the Tsinghua University Initiative Scientific Research Program (2012Z02134) and the Thousand Young Talents Program (20121770071). The authors are grateful to the entire Martini Research group for careful review and helpful feedback on the manuscript.

- <sup>1</sup>C. M. Mate, G. M. McClelland, R. Erlandsson, and S. Chiang, *Phys. Rev. Lett.* **59**, 1942 (1987).
- <sup>2</sup>Q. Li, Y. Dong, D. Perez, A. Martini, and R. W. Carpick, *Phys. Rev. Lett.* **106**, 126101 (2011).
- <sup>3</sup>I. L. Singer, *J. Vac. Sci. Technol. A* **12**, 2605 (1994).
- <sup>4</sup>B. Bhushan, J. N. Israelachvili, and U. Landman, *Nature* **374**, 607 (1995).
- <sup>5</sup>R. W. Carpick and M. Salmeron, *Chem. Rev.* **97**, 1163 (1997).
- <sup>6</sup>G. V. Dedkov, *Physica Status Solidi A* **179**, 3 (2000).
- <sup>7</sup>E. Gnecco, R. Bennewitz, T. Gyalog, and E. Meyer, *J. Phys.: Condens. Matter* **13**, 619 (2001).
- <sup>8</sup>M. Urbakh, J. Klafter, D. Gourdon, and J. Israelachvili, *Nature* **430**, 525 (2004).
- <sup>9</sup>O. M. Braun and A. G. Naumovets, *Surf. Sci. Rep.* **60**, 79 (2006).
- <sup>10</sup>I. Szlufarska, M. Chandross, and R. W. Carpick, *J. Phys. D: Appl. Phys.* **41**, 123001 (2008).
- <sup>11</sup>H. Hölscher, A. Schirmeisen, and U. D. Schwarz, *Phil. Trans. R. Soc. A* **366**, 1383 (2008).
- <sup>12</sup>H. J. Kim and D. E. Kim, *Inter. J. Prec. Eng. Manufac.* **10**, 141 (2009).
- <sup>13</sup>Y. Dong, A. Vadakkepat, and A. Martini, *Tribol. Lett.* **44**, 367 (2011).
- <sup>14</sup>J. E. Jones, *Proc. R. Soc. London, Ser. A* **106**, 463 (1924).
- <sup>15</sup>A. Warshel and S. Lifson, *J. Chem. Phys.* **53**, 582 (1970).
- <sup>16</sup>B. Luan and M. Robbins, *Nature* **435**, 929 (2005).
- <sup>17</sup>B. Luan and M. O. Robbins, *Phys. Rev. E* **74**, 026111 (2006).
- <sup>18</sup>M. Cieplak, E. D. Smith, and M. O. Robbins, *Science* **265**, 1209 (1994).
- <sup>19</sup>L. C. Allen, J. F. Capitani, G. A. Kolks, and G. D. Sproul, *J. Mol. Struct.* **300**, 647 (1993).
- <sup>20</sup>C. Kittel and P. McEuen, *Introduction to Solid State Physics* (Wiley, New York, 1976), Vol. 7.
- <sup>21</sup>M. S. Daw and M. I. Baskes, *Phys. Rev. B* **29**, 6443 (1984).
- <sup>22</sup>S. M. Foiles, M. I. Baskes, and M. S. Daw, *Phys. Rev. B* **33**, 7983 (1986).
- <sup>23</sup>M. S. Daw, S. M. Foiles, and M. I. Baskes, *Mater. Sci. Rep.* **9**, 251 (1993).
- <sup>24</sup>U. Landman, W. D. Luedtke, N. A. Burnham, and R. J. Colton, *Science* **248**, 454 (1990).
- <sup>25</sup>J. A. Nieminen, A. P. Sutton, and J. B. Pethica, *Acta Metall.* **40**, 2503 (1992).
- <sup>26</sup>A. Buldum, S. Ciraci, and I. P. Batra, *Phys. Rev. B* **57**, 2468 (1998).
- <sup>27</sup>R. Komanduri, N. Chandrasekaran, and L. M. Raff, *Phys. Rev. B* **61**, 14007 (2000).
- <sup>28</sup>M. H. Cho, S. J. Kim, D. S. Lim, and H. Jang, *Wear* **259**, 1392 (2005).
- <sup>29</sup>H. J. Kim, A. Emge, R. E. Winter, P. T. Keightley, W. K. Kim, M. L. Falk, and D. A. Rigney, *Acta Mater.* **57**, 5270 (2009).
- <sup>30</sup>N. N. Gosvami, M. Feldmann, J. Peguiron, M. Moseler, A. Schirmeisen, and R. Bennewitz, *Phys. Rev. Lett.* **107**, 144303 (2011).
- <sup>31</sup>M. I. Baskes, J. S. Nelson, and A. F. Wright, *Phys. Rev. B* **40**, 6085 (1989).
- <sup>32</sup>F. H. Stillinger and T. A. Weber, *Phys. Rev. B* **31**, 5262 (1985).
- <sup>33</sup>J. Tersoff, *Phys. Rev. B* **37**, 6991 (1988).
- <sup>34</sup>D. W. Brenner, *Phys. Rev. B* **42**, 9458 (1990).
- <sup>35</sup>S. J. Stuart, A. B. Tutein, and J. A. Harrison, *J. Chem. Phys.* **112**, 6472 (2000).
- <sup>36</sup>A. C. T. Van Duin, S. Dasgupta, F. Lorant, and W. A. Goddard III, *J. Phys. Chem. A* **105**, 9396 (2001).
- <sup>37</sup>J. A. Harrison, C. T. White, R. J. Colton, and D. W. Brenner, *Phys. Rev. B* **46**, 9700 (1992).
- <sup>38</sup>J. A. Harrison, R. J. Colton, C. T. White, and D. W. Brenner, *Wear* **168**, 127 (1993).
- <sup>39</sup>J. Han, A. Globus, R. Jaffe, and G. Deardorff, *Nanotechnology* **8**, 95 (1997).
- <sup>40</sup>M. J. Brukman, G. Gao, R. J. Nemanich, and J. A. Harrison, *J. Phys. Chem. C* **112**, 9358 (2008).
- <sup>41</sup>G. Gao, R. J. Cannara, R. W. Carpick, and J. A. Harrison, *Langmuir* **23**, 5394 (2007).
- <sup>42</sup>E. Gnecco, R. Bennewitz, T. Gyalog, C. Loppacher, M. Bammerlin, E. Meyer, and H. J. Güntherodt, *Phys. Rev. Lett.* **84**, 1172 (2000).
- <sup>43</sup>A. Socoliu, R. Bennewitz, E. Gnecco, and E. Meyer, *Phys. Rev. Lett.* **92**, 134301 (2004).
- <sup>44</sup>S. Maier, E. Gnecco, A. Baratoff, R. Bennewitz, and E. Meyer, *Phys. Rev. B* **78**, 045432 (2008).
- <sup>45</sup>S. Maier, Y. Sang, T. Filletter, M. Grant, R. Bennewitz, E. Gnecco, and E. Meyer, *Phys. Rev. B* **72**, 245418 (2005).
- <sup>46</sup>U. Wyder, A. Baratoff, E. Meyer, L. N. Kantorovich, J. David, S. Maier, T. Filletter, and R. Bennewitz, *J. Vac. Sci. Technol. B* **25**, 1547 (2007).
- <sup>47</sup>R. Bennewitz, T. Gyalog, M. Guggisberg, M. Bammerlin, E. Meyer, and H. J. Güntherodt, *Phys. Rev. B* **60**, 11301 (1999).
- <sup>48</sup>M. Dienwiebel, G. S. Verhoeven, N. Pradeep, J. W. M. Frenken, J. A. Heimberg, and H. W. Zandbergen, *Phys. Rev. Lett.* **92**, 126101 (2004).
- <sup>49</sup>N. N. Gosvami, T. Filletter, P. Egberts, and R. Bennewitz, *Tribol. Lett.* **39**, 19 (2010).
- <sup>50</sup>P. L. Williams, Y. Mishin, and J. C. Hamilton, *Modelling Simul. Mater. Sci. Eng.* **14**, 817 (2006).
- <sup>51</sup>F. Apostol and Y. Mishin, *Phys. Rev. B* **83**, 054116 (2011).
- <sup>52</sup>J. Yu, S. B. Sinnott, and S. R. Phillpot, *Phys. Rev. B* **75**, 085311 (2007).
- <sup>53</sup>T. Shan, B. Devine, T. Kemper, S. Sinnott, and S. Phillpot, *Phys. Rev. B* **81**, 125328 (2010).
- <sup>54</sup>C. A. Becker, in *Models, Databases, and Simulation Tools Needed for the Realization of Integrated Computational Materials Engineering: Proceedings of the Symposium* (ASM International, Houston, TX, 2011), p. 91.
- <sup>55</sup>E. B. Tadmor, R. S. Elliott, J. P. Sethna, R. E. Miller, and C. A. Becker, *JOM* **63**, 17 (2011).
- <sup>56</sup>M. R. Sørensen, K. W. Jacobsen, and P. Stoltze, *Phys. Rev. B* **53**, 2101 (1996).
- <sup>57</sup>Y. Dong, Q. Li, J. Wu, and A. Martini, *Modell. Simul. Mater. Sci. Eng.* **19**, 065003 (2011).
- <sup>58</sup>U. Harten, A. M. Lahee, J. P. Toennies, and C. Wöll, *Phys. Rev. Lett.* **54**, 2619 (1985).
- <sup>59</sup>T. Filletter and R. Bennewitz, *Phys. Rev. B* **81**, 155412 (2010).
- <sup>60</sup>P. Steiner, E. Gnecco, T. Filletter, N. N. Gosvami, S. Maier, E. Meyer, and R. Bennewitz, *Tribol. Lett.* **39**, 321 (2010).
- <sup>61</sup>Q. Li, Y. Dong, A. Martini, and R. W. Carpick, *Tribol. Lett.* **43**, 369 (2011).
- <sup>62</sup>M. I. HafTEL, *Phys. Rev. B* **48**, 2611 (1993).

- <sup>63</sup>T. Müller, M. Lohrmann, T. Kässer, O. Marti, J. Mlynek, and G. Krausch, *Phys. Rev. Lett.* **79**, 5066 (1997).
- <sup>64</sup>F. Hausen, M. Nielinger, S. Ernst, and H. Baltruschat, *Electrochim. Acta* **53**, 6058 (2008).
- <sup>65</sup>H. Hölscher, D. Ebeling, and U. D. Schwarz, *Phys. Rev. Lett.* **101**, 246105 (2008).
- <sup>66</sup>P. Steiner, E. Gnecco, F. Krok, J. Budzioch, L. Walczak, J. Konior, M. Szymonski, and E. Meyer, *Phys. Rev. Lett.* **106**, 186104 (2011).
- <sup>67</sup>Y. Dong, X. Z. Liu, P. Egbert, Z. Ye, R. W. Carpick, and A. Martini, *Tribol. Lett.* (in press).
- <sup>68</sup>R. L. Schwoebel and E. J. Shipsey, *J. Appl. Phys.* **37**, 3682 (1966).
- <sup>69</sup>G. Ehrlich, *J. Chem. Phys.* **44**, 1050 (1966).
- <sup>70</sup>M. Hirano, K. Shinjo, R. Kaneko, and Y. Murata, *Phys. Rev. Lett.* **67**, 2642 (1991).
- <sup>71</sup>M. H. Müser, *Europhys. Lett.* **66**, 97 (2004).
- <sup>72</sup>J. M. Martin, C. Donnet, T. Le Mogne, and T. Epicier, *Phys. Rev. B* **48**, 10583 (1993).
- <sup>73</sup>M. Hirano, K. Shinjo, R. Kaneko, and Y. Murata, *Phys. Rev. Lett.* **78**, 1448 (1997).
- <sup>74</sup>A. Crossley, E. H. Kisi, J. W. Summers, and S. Myhra, *J. Phys. D: Appl. Phys.* **32**, 632 (1999).
- <sup>75</sup>A. P. Merkle and L. D. Marks, *Tribol. Lett.* **26**, 73 (2007).
- <sup>76</sup>J. M. B. Lopes dos Santos, N. M. R. Peres, and A. H. Castro Neto, *Phys. Rev. Lett.* **99**, 256802 (2007).
- <sup>77</sup>V. A. Ivanov and Y. Mishin, *Phys. Rev. B* **78**, 064106 (2008).
- <sup>78</sup>K. L. Johnson, *Contact Mechanics* (Cambridge Univ. Press, Cambridge, England, 1987).
- <sup>79</sup>J. A. Hurtado and K. S. Kim, *Phil. Trans. R. Soc. A* **455**, 3363 (1999).
- <sup>80</sup>J. A. Hurtado and K. S. Kim, *Phil. Trans. R. Soc. A* **455**, 3385 (1999).
- <sup>81</sup>Y. Gao, *J. Mech. Phys. Sol.* **58**, 2023 (2010).
- <sup>82</sup>R. M. Overney, H. Takano, M. Fujihira, W. Paulus, and H. Ringsdorf, *Phys. Rev. Lett.* **72**, 3546 (1994).
- <sup>83</sup>Y. Qi, Y. T. Cheng, T. Çağın, and W. A. Goddard III, *Phys. Rev. B* **66**, 085420 (2002).
- <sup>84</sup>J. Y. Park, D. F. Ogletree, M. Salmeron, R. A. Ribeiro, P. C. Canfield, C. J. Jenks, and P. A. Thiel, *Science* **309**, 1354 (2005).
- <sup>85</sup>A. E. Filippov, A. Vanossi, and M. Urbakh, *Phys. Rev. Lett.* **104**, 74302 (2010).
- <sup>86</sup>M. Campione and E. Fumagalli, *Phys. Rev. Lett.* **105**, 166103 (2010).
- <sup>87</sup>C. Tourek and S. Sundararajan, *Microsc. Microanal.* **15**, 290 (2009).
- <sup>88</sup>E. Riedo, E. Gnecco, R. Bennewitz, E. Meyer, and H. Brune, *Phys. Rev. Lett.* **91**, 84502 (2003).
- <sup>89</sup>K. L. Johnson and J. Woodhouse, *Tribol. Lett.* **5**, 155 (1998).
- <sup>90</sup>S. N. Medyanik, W. K. Liu, I. H. Sung, and R. W. Carpick, *Phys. Rev. Lett.* **97**, 136106 (2006).
- <sup>91</sup>R. W. Carpick, D. F. Ogletree, and M. Salmeron, *Appl. Phys. Lett.* **70**, 1548 (1997).
- <sup>92</sup>G. Binnig, C. F. Quate, and C. Gerber, *Phys. Rev. Lett.* **56**, 930 (1986).
- <sup>93</sup>J. L. Hutter and J. Bechhoefer, *Rev. Sci. Instrum.* **64**, 1868 (1993).
- <sup>94</sup>M. Munz, *J. Phys. D: Appl. Phys.* **43**, 063001 (2010).
- <sup>95</sup>D. F. Ogletree, R. W. Carpick, and M. Salmeron, *Rev. Sci. Instrum.* **67**, 3298 (1996).
- <sup>96</sup>M. A. Lantz, S. J. Oshea, A. C. F. Hoole, and M. E. Welland, *Appl. Phys. Lett.* **70**, 970 (1997).
- <sup>97</sup>O. Piétrement, J. L. Beaudoin, and M. Troyon, *Tribol. Lett.* **7**, 213 (1999).
- <sup>98</sup>M. A. Lantz, S. J. O'shea, M. E. Welland, and K. L. Johnson, *Phys. Rev. B* **55**, 10776 (1997).
- <sup>99</sup>P. Reimann and M. Evstigneev, *New J. Phys.* **7**, 25 (2005).
- <sup>100</sup>S. Y. Krylov, J. A. Dijksman, W. A. Van Loo, and J. W. M. Frenken, *Phys. Rev. Lett.* **97**, 166103 (2006).
- <sup>101</sup>D. G. Abel, S. Y. Krylov, and J. W. M. Frenken, *Phys. Rev. Lett.* **99**, 166102 (2007).
- <sup>102</sup>S. Y. Krylov and J. W. M. Frenken, *New J. Phys.* **9**, 398 (2007).
- <sup>103</sup>S. Y. Krylov and J. W. M. Frenken, *Phys. Rev. B* **80**, 235435 (2009).
- <sup>104</sup>Z. Tshiprut, A. E. Filippov, and M. Urbakh, *J. Phys.: Condens. Matter* **20**, 354002 (2008).
- <sup>105</sup>J. Shimizu, H. Eda, M. Yoritsune, and E. Ohmura, *Nanotechnology* **9**, 118 (1998).
- <sup>106</sup>Y. Leng and S. Jiang, *Tribol. Lett.* **11**, 111 (2001).
- <sup>107</sup>R. Smith, D. Mulliah, S. D. Kenny, E. McGee, A. Richter, and M. Gruner, *Wear* **259**, 459 (2005).
- <sup>108</sup>K. Matsushita, H. Matsukawa, and N. Sasaki, *Solid State Commun.* **136**, 51 (2005).
- <sup>109</sup>W. K. Kim and M. L. Falk, *Phys. Rev. B* **80**, 235428 (2009).
- <sup>110</sup>W. K. Kim and M. L. Falk, *Phys. Rev. B* **84**, 165422 (2011).
- <sup>111</sup>Y. Dong, D. Perez, A. F. Voter, and A. Martini, *Tribol. Lett.* **42**, 99 (2011).
- <sup>112</sup>A. P. Merkle and L. D. Marks, *Appl. Phys. Lett.* **90**, 064101 (2007).
- <sup>113</sup>A. P. Merkle and L. D. Marks, *Wear* **265**, 1864 (2008).
- <sup>114</sup>K. Ananthshewara and M. S. Bobji, *Tribol. Int.* **43**, 1099 (2010).
- <sup>115</sup>D. Dietzel, C. Ritter, T. Mönnighoff, H. Fuchs, A. Schirmeisen, and U. D. Schwarz, *Phys. Rev. Lett.* **101**, 125505 (2008).
- <sup>116</sup>H. Hertz, *J. Reine Angew. Math* **92**, 156 (1881).
- <sup>117</sup>K. L. Johnson, K. Kendall, and A. D. Roberts, *Phil. Trans. R. Soc. A* **324**, 301 (1971).
- <sup>118</sup>B. V. Derjaguin, V. M. Muller, and Y. P. Toporov, *J. Colloid Interface Sci.* **53**, 314 (1975).
- <sup>119</sup>D. Tabor, *J. Colloid Interface Sci.* **58**, 2 (1977).
- <sup>120</sup>D. Maugis, *J. Colloid Interface Sci.* **150**, 243 (1992).
- <sup>121</sup>U. D. Schwarz, O. Zwörner, P. Köster, and R. Wiesendanger, *Phys. Rev. B* **56**, 6987 (1997).
- <sup>122</sup>R. W. Carpick, D. Frank Ogletree, and Miquel Salmeron, *J. Colloid Interface Sci.* **211**, 395 (1999).
- <sup>123</sup>K. L. Johnson, *Tribol. Int.* **31**, 413 (1998).
- <sup>124</sup>Y. Mo, K. T. Turner, and I. Szlufarska, *Nature* **457**, 1116 (2009).
- <sup>125</sup>S. Cheng and M. O. Robbins, *Tribol. Lett.* **39**, 329 (2010).
- <sup>126</sup>M. Enachescu, R. Van den Oetelaar, R. W. Carpick, D. F. Ogletree, C. Flipse, and M. Salmeron, *Tribol. Lett.* **7**, 73 (1999).
- <sup>127</sup>F. Lancon, J. Ye, D. Caliste, T. Radetic, A. M. Minor, and U. Dahmen, *Nano Lett.* **10**, 695 (2010).
- <sup>128</sup>Z. Liu, J. Yang, F. Grey, J. Z. Liu, Y. Liu, Y. Wang, Y. Yang, Y. Cheng, and Q. Zheng, *Phys. Rev. Lett.* **108**, 205503 (2012).
- <sup>129</sup>J. Liu, J. K. Notbohm, R. W. Carpick, and K. T. Turner, *ACS Nano* **4**, 3763 (2010).
- <sup>130</sup>J. Gao, W. D. Luedtke, D. Gourdon, M. Ruths, J. N. Israelachvili, and U. Landman, *J. Phys. Chem. B* **108**, 3410 (2004).
- <sup>131</sup>O. Pietrement and M. Troyon, *Langmuir* **17**, 6540 (2001).
- <sup>132</sup>L. Wenning and M. H. Müser, *Europhys. Lett.* **54**, 693 (2001).
- <sup>133</sup>C. Greiner, J. R. Felts, Z. Dai, W. P. King, and R. W. Carpick, *Nano Lett.* **10**, 4640 (2010).
- <sup>134</sup>L. Jansen, H. Hölscher, H. Fuchs, and A. Schirmeisen, *Phys. Rev. Lett.* **104**, 256101 (2010).
- <sup>135</sup>A. Schirmeisen, L. Jansen, H. Hölscher, and H. Fuchs, *Appl. Phys. Lett.* **88**, 123108 (2006).
- <sup>136</sup>X. Zhao, S. Phillipot, W. G. Sawyer, S. B. Sinnott, and S. S. Perry, *Phys. Rev. Lett.* **102**, 186102 (2009).
- <sup>137</sup>I. Barel, M. Urbakh, L. Jansen, and A. Schirmeisen, *Phys. Rev. Lett.* **104**, 66104 (2010).
- <sup>138</sup>I. Barel, M. Urbakh, L. Jansen, and A. Schirmeisen, *Phys. Rev. B* **84**, 115417 (2011).
- <sup>139</sup>V. Kapila, P. A. Deymier, and S. Raghavan, *Modell. Simul. Mater. Sci. Eng.* **14**, 283 (2006).
- <sup>140</sup>L. Prandtl, *Z. Angew. Math. Mech.* **8**, 85 (1928).
- <sup>141</sup>G. A. Tomlinson, *Philos. Mag.* **7**, 905 (1929).
- <sup>142</sup>P. Hanggi, P. Talkner, and M. Borkovec, *Rev. Mod. Phys.* **62**, 251 (1990).
- <sup>143</sup>Y. Sang, M. Dubé, and M. Grant, *Phys. Rev. Lett.* **87**, 174301 (2001).
- <sup>144</sup>O. J. Furlong, S. J. Manzi, V. D. Pereyra, V. Bustos, and W. T. Tysoe, *Phys. Rev. B* **80**, 153408 (2009).
- <sup>145</sup>Y. Dong, D. Perez, H. Gao, and A. Martini, *J. Phys.: Condens. Matter* **24**, 265001 (2012).
- <sup>146</sup>A. E. Filippov, J. Klafter, and M. Urbakh, *Phys. Rev. Lett.* **92**, 135503 (2004).
- <sup>147</sup>A. Labuda, M. Lysy, W. Paul, Y. Miyahara, P. Grüter, R. Bennewitz, and M. Sutton, *Phys. Rev. E* **86**, 031104 (2012).
- <sup>148</sup>A. Labuda, M. Lysy, and P. Grüter, *Appl. Phys. Lett.* **101**, 113105 (2012).
- <sup>149</sup>Y. Dong, H. Gao, and A. Martini, *Europhys. Lett.* **98**, 16002 (2012).
- <sup>150</sup>S. Sinnott, S. J. Heo, D. Brenner, and J. Harrison, in *Springer Handbook of Nanotechnology* (Springer, New York, 2007), pp. 1051–1106.
- <sup>151</sup>M. Kisiel, E. Gnecco, U. Gysin, L. Marot, S. Rast, and E. Meyer, *Nature Mater.* **10**, 119 (2011).
- <sup>152</sup>A. Benassi, A. Vanossi, G. E. Santoro, and E. Tosatti, *Phys. Rev. B* **82**, 081401 (2010).
- <sup>153</sup>A. Benassi, A. Vanossi, G. E. Santoro, and E. Tosatti, *Tribol. Lett.* **48**, 41 (2012).

- <sup>154</sup>S. Sills and R. M. Overney, *Phys. Rev. Lett.* **91**, 95501 (2003).
- <sup>155</sup>J. Chen, I. Ratera, J. Y. Park, and M. Salmeron, *Phys. Rev. Lett.* **96**, 236102 (2006).
- <sup>156</sup>N. S. Tambe and B. Bhushan, *Nanotechnology* **16**, 2309 (2005).
- <sup>157</sup>C. Greiner, J. Felts, Z. Dai, W. P. King, and R. W. Carpick, *ACS Nano* **6**, 4305 (2012).
- <sup>158</sup>N. S. Tambe and B. Bhushan, *J. Phys. D: Appl. Phys.* **38**, 764 (2005).
- <sup>159</sup>Z. Tao and B. Bhushan, *Rev. Sci. Instrum.* **77**, 103705 (2006).
- <sup>160</sup>M. H. Müser, *Phys. Rev. Lett.* **89**, 224301 (2002).
- <sup>161</sup>A. F. Voter, *Phys. Rev. Lett.* **78**, 3908 (1997).
- <sup>162</sup>M. R. Sørensen and A. F. Voter, *J. Chem. Phys.* **112**, 9599 (2000).
- <sup>163</sup>A. F. Voter, *Phys. Rev. B* **57**, 13985 (1998).
- <sup>164</sup>S. Hara and J. Li, *Phys. Rev. B* **82**, 184114 (2010).
- <sup>165</sup>D. Perez, B. P. Uberuaga, Y. Shim, J. G. Amar, and A. F. Voter, *Ann. Rep. Comp. Chem.* **5**, 79 (2009).
- <sup>166</sup>Y. Mishin, A. Suzuki, B. P. Uberuaga, and A. F. Voter, *Phys. Rev. B* **75**, 224101 (2007).
- <sup>167</sup>A. Martini, Y. Dong, D. Perez, and A. F. Voter, *Tribol. Lett.* **36**, 63 (2009).
- <sup>168</sup>W. K. Kim and M. L. Falk, *Modell. Simul. Mater. Sci. Eng.* **18**, 034003 (2010).
- <sup>169</sup>B. P. Uberuaga, S. J. Stuart, and A. F. Voter, *Phys. Rev. B* **75**, 014301 (2007).
- <sup>170</sup>Y. Dong, Q. Li, R. W. Carpick, and A. Martini, *Tribol. Lubr. Tech.* Feb. 17 (2012).
- <sup>171</sup>A. F. Voter, F. Montalenti, and T. C. Germann, *Ann. Rev. Mater. Res.* **32**, 321 (2002).
- <sup>172</sup>Q. Li, T. E. Tullis, D. Goldsby, and R. W. Carpick, *Nature* **480**, 233 (2011).
- <sup>173</sup>D. Dietzel, M. Feldmann, H. Fuchs, U. D. Schwarz, and A. Schirmeisen, *Appl. Phys. Lett.* **95**, 053104 (2009).
- <sup>174</sup>D. Perez, Y. Dong, A. Martini, and A. F. Voter, *Phys. Rev. B* **81**, 245415 (2010).
- <sup>175</sup>Y. Liu and I. Szlufarska, *Phys. Rev. Lett.* **109**, 186102 (2012).
- <sup>176</sup>Z. Deng, A. Smolyanitsky, Q. Li, X. Q. Feng, and R. J. Cannara, *Nature Mater.* **11**, 1032 (2012).
- <sup>177</sup>S. Kwon, J. H. Ko, K. J. Jeon, Y. H. Kim, and J. Y. Park, *Nano Lett.* **12**, 6043 (2012).
- <sup>178</sup>M. Garvey, O. J. Furlong, M. Weinert, and W. T. Tysoe, *J. Phys.: Condens. Matter* **23**, 265003 (2011).
- <sup>179</sup>M. Garvey, M. Weinert, and W. T. Tysoe, *Wear* **274**, 281 (2012).
- <sup>180</sup>M. Garvey, M. Weinert, and W. T. Tysoe, *Tribol. Lett.* **44**, 67 (2011).
- <sup>181</sup>L. F. Wang, T. B. Ma, Y. Z. Hu, and H. Wang, *Phys. Rev. B* **86**, 125436 (2012).
- <sup>182</sup>J. Wang, F. Wang, J. Li, S. Wang, Y. Song, Q. Sun, and Y. Jia, *Tribol. Lett.* **48**, 255 (2012).